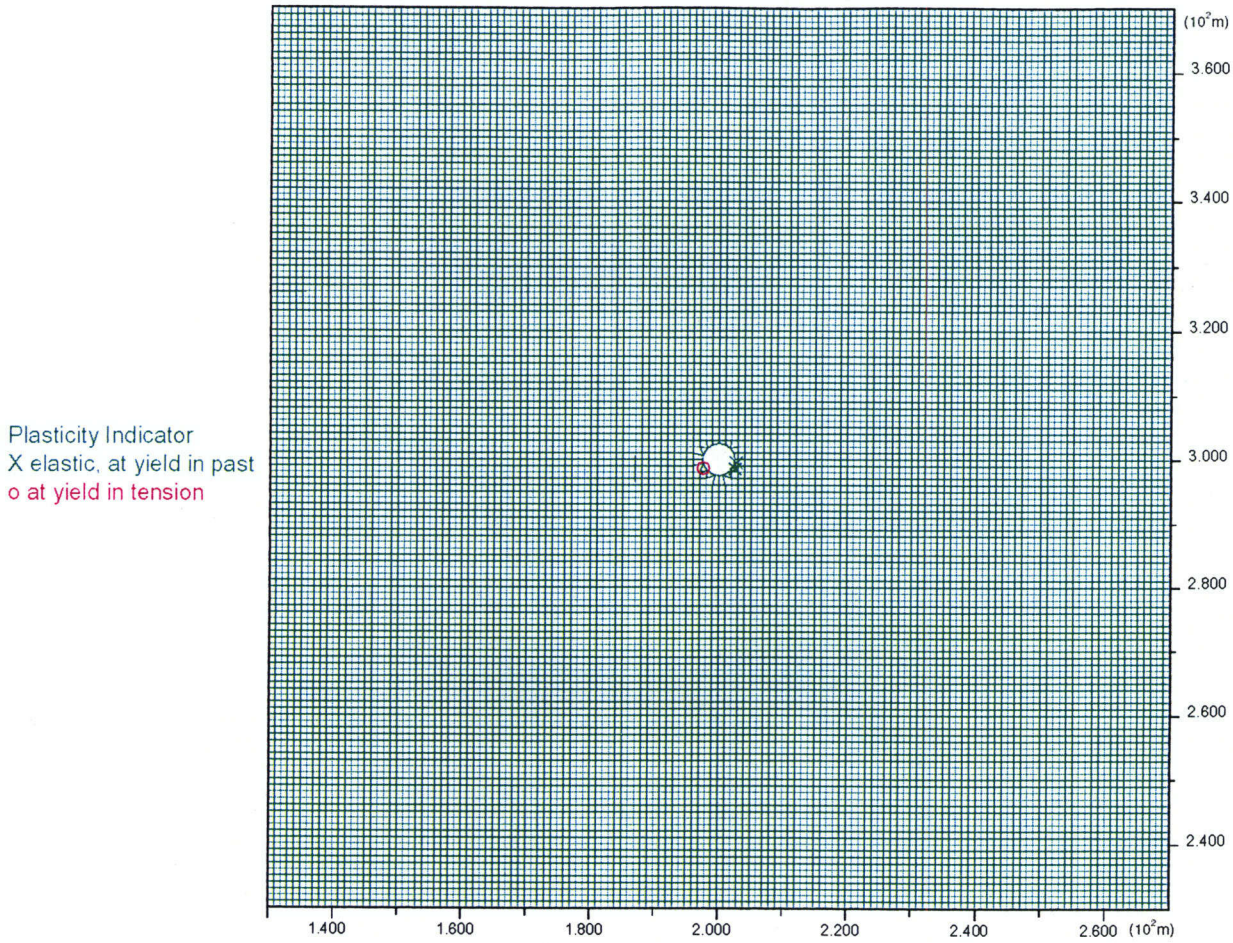

(a) After 3 Months of Heating

Figure 4-14. Extent of yielding in rock as a function of time for Sensitivity Case 4 with Temperature Option 1

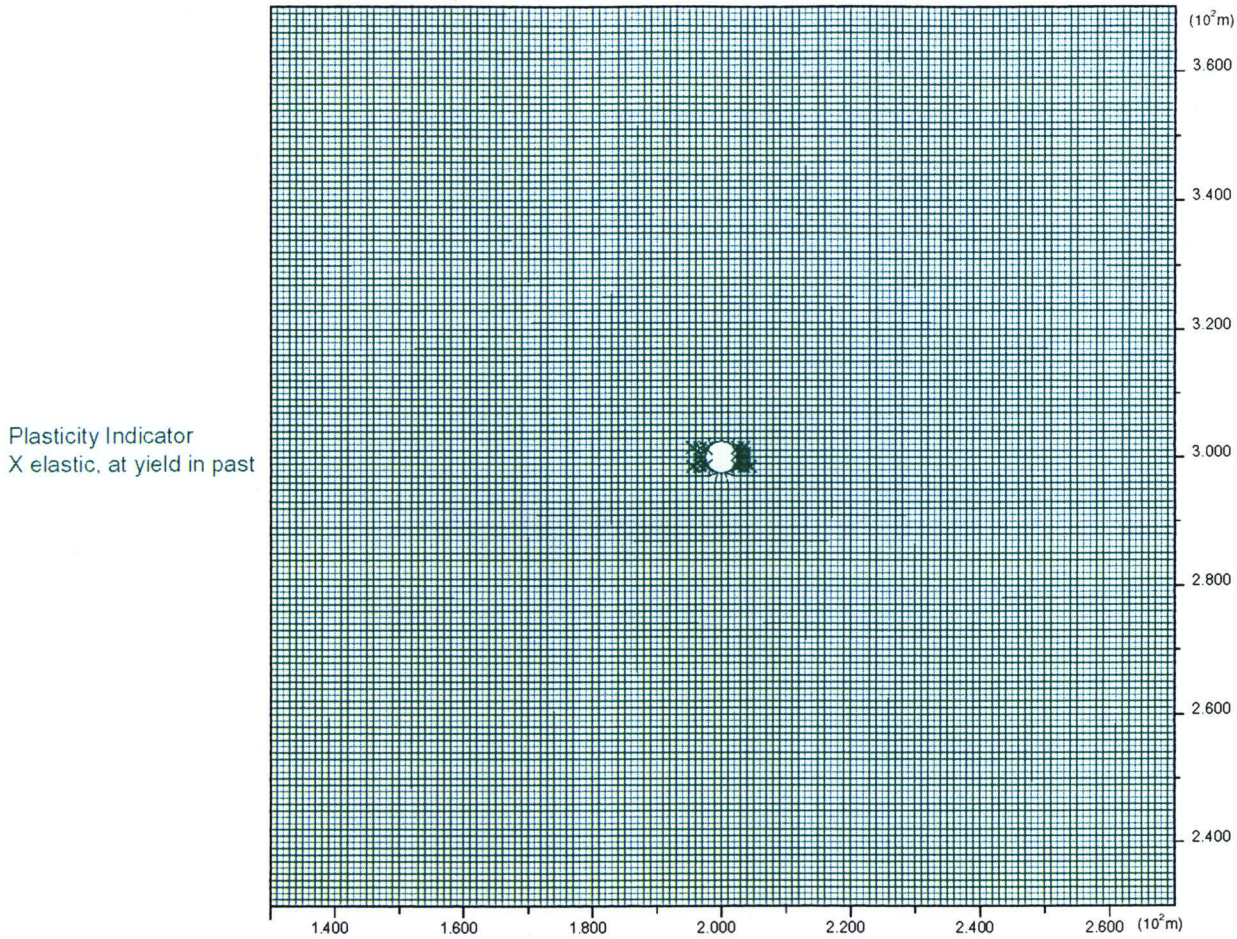

(b) After 1 Year of Heating

Figure 4-14. Extent of yielding in rock as a function of time for Sensitivity Case 4 with Temperature Option 1 (cont'd)

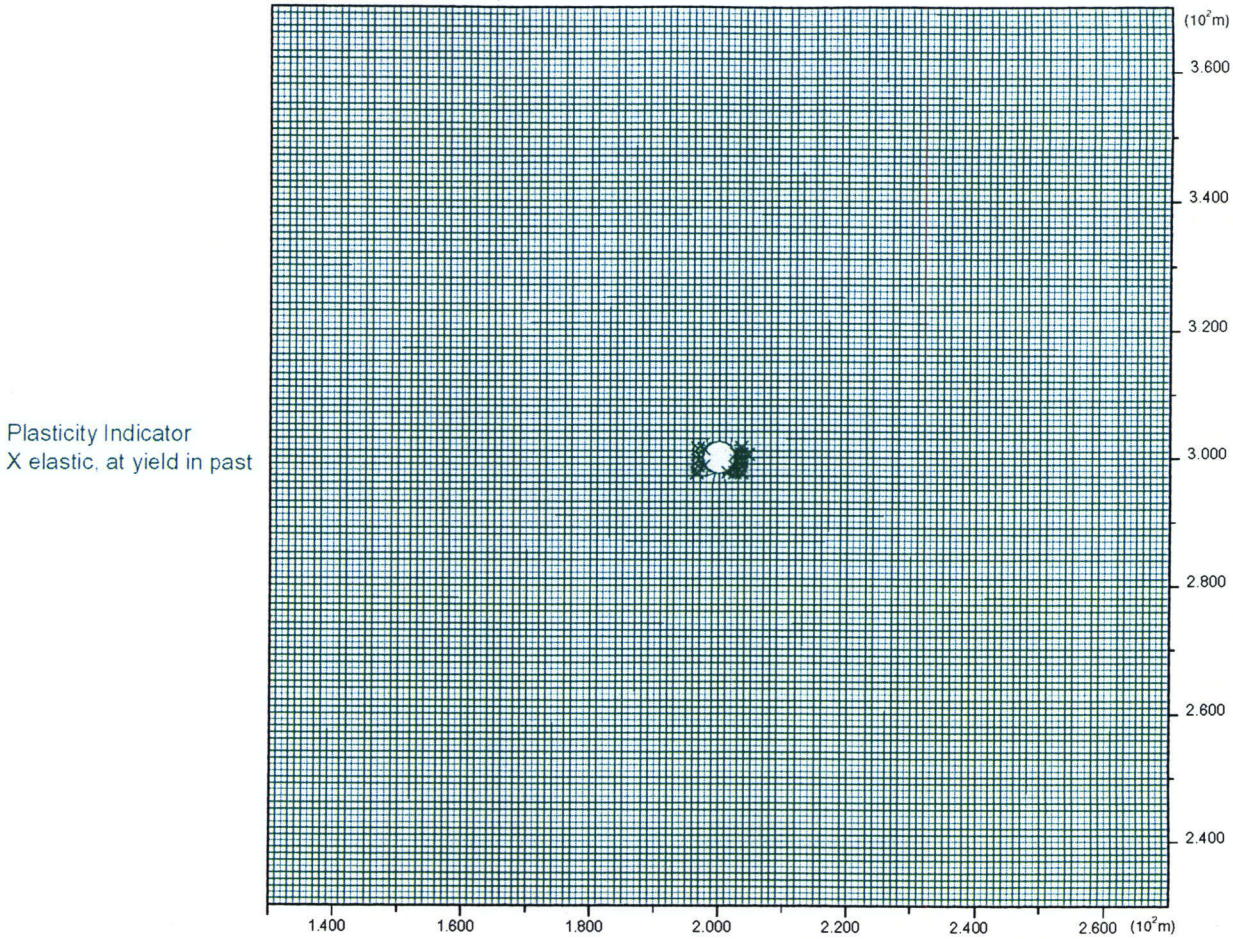

(c) After 4 Years of Heating

Figure 4-14. Extent of yielding in rock as a function of time for Sensitivity Case 4 with Temperature Option 1 (cont'd)

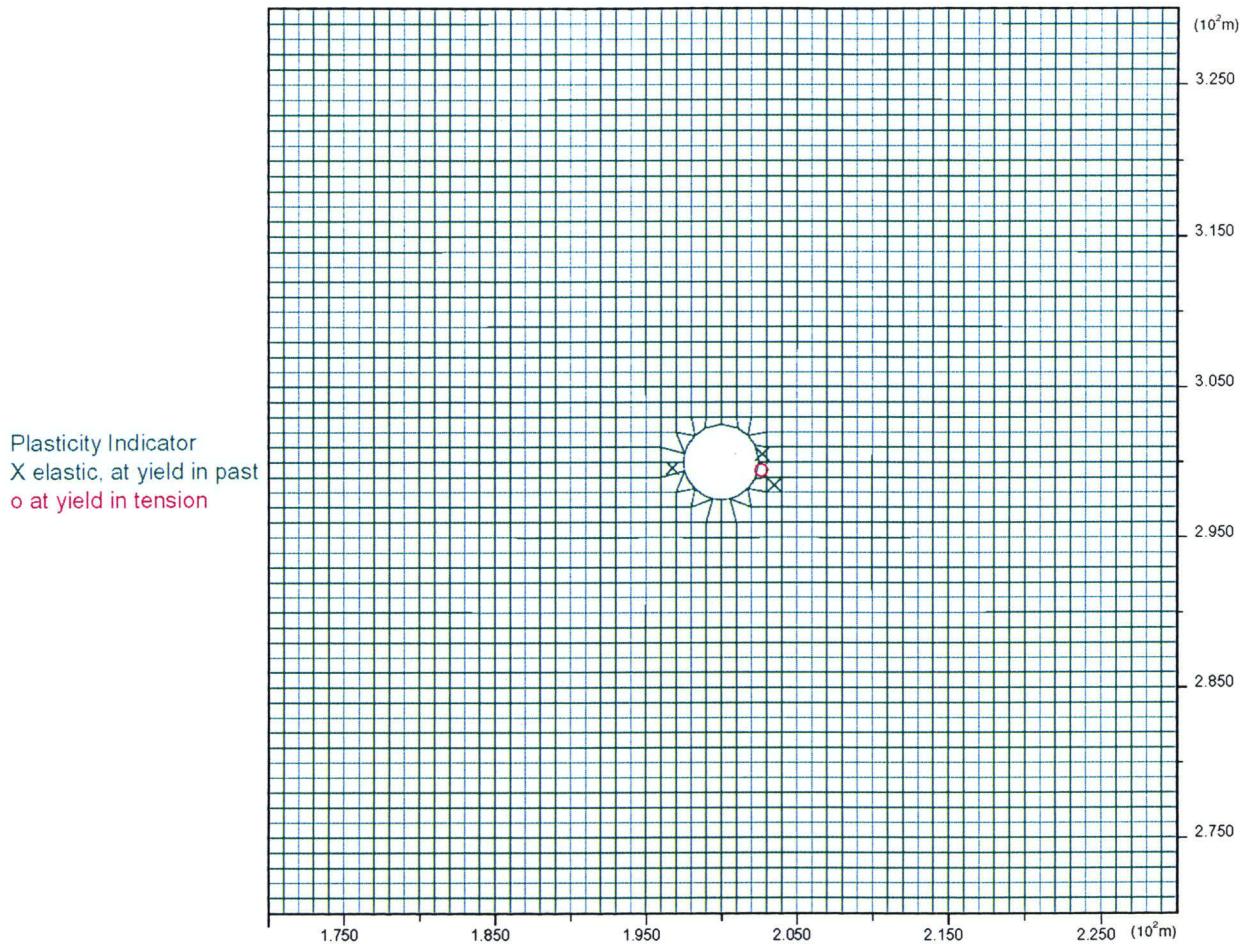

(a) After 3 Months of Heating

Figure 4-15. Extent of yielding in rock as a function of time for Sensitivity Case 4 with Temperature Option 2

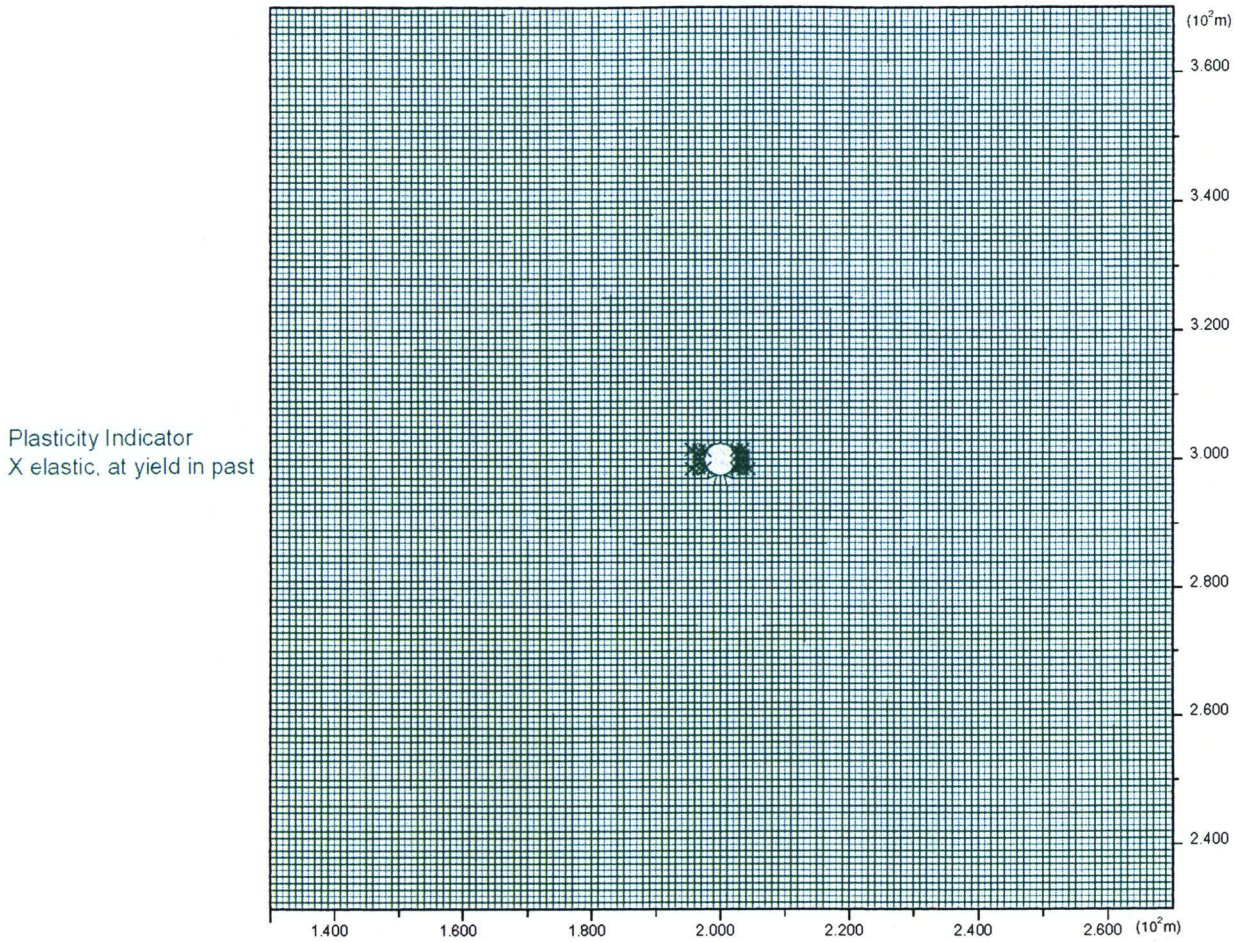

(b) After 4 Years of Heating

Figure 4-15. Extent of yielding in rock as a function of time for Sensitivity Case 4 with Temperature Option 2 (cont'd)

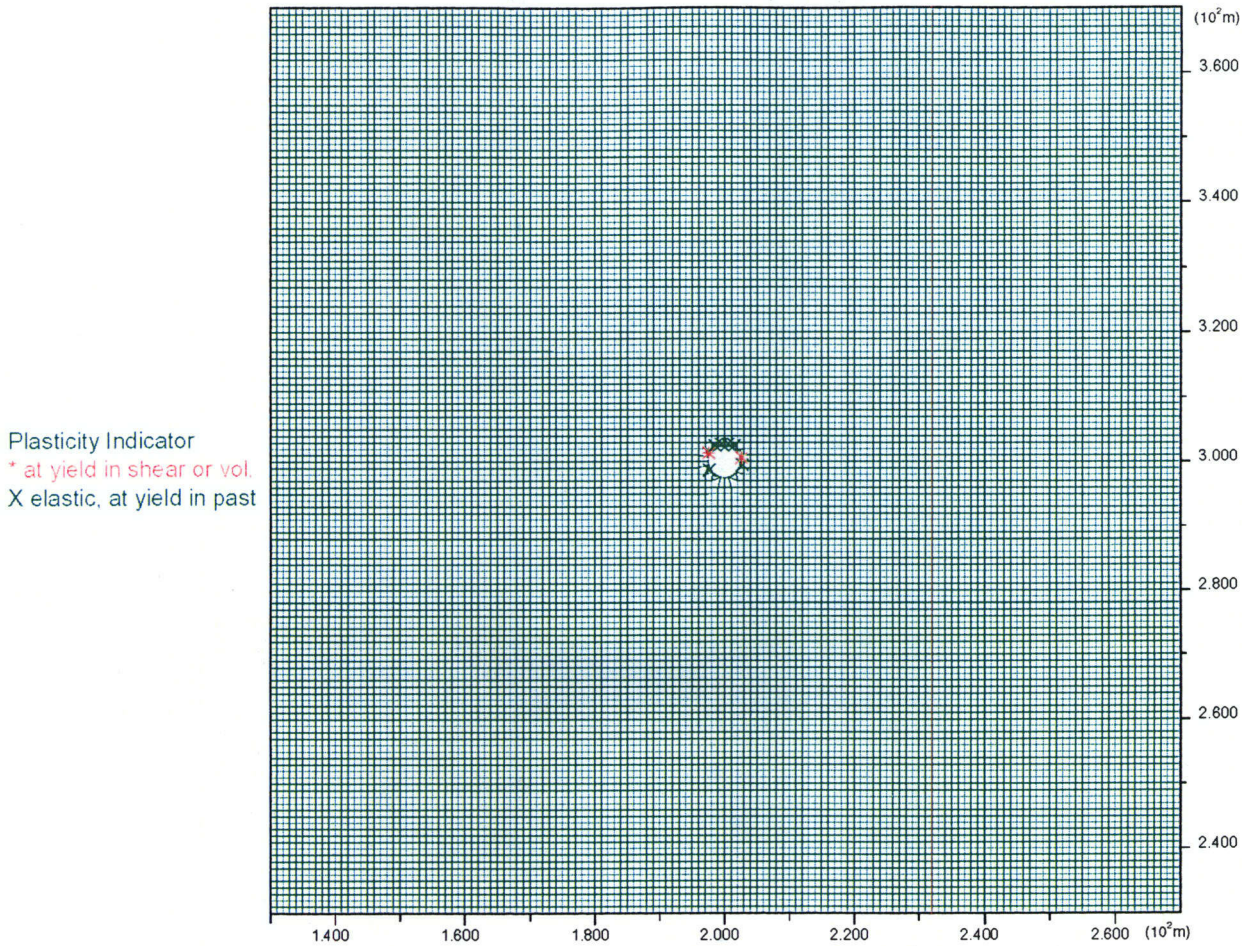

(a) Rock-Mass Quality Category 1 (Sensitivity Case 5)

Figure 4-16. Effects of drift excavation on yielding of rock

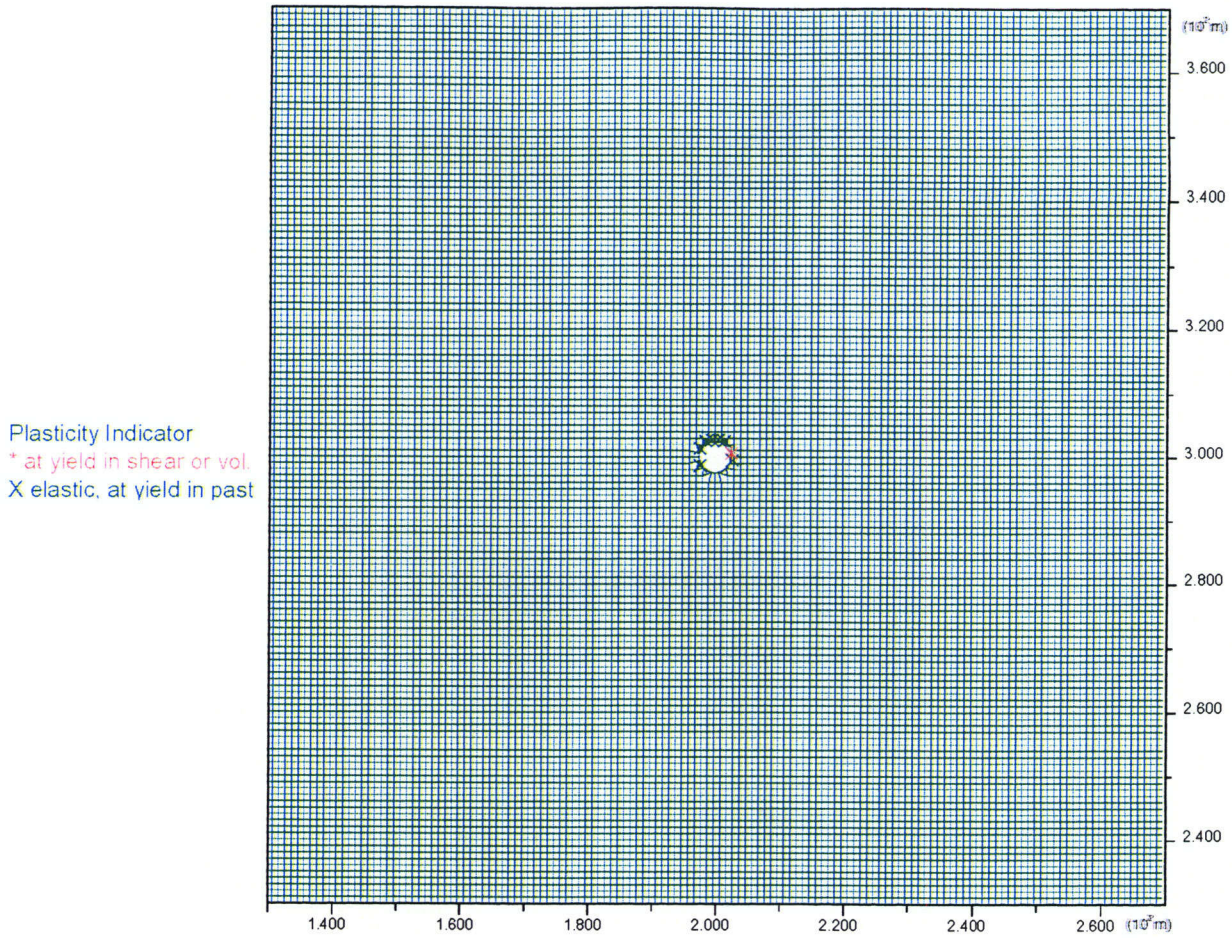

(b) Rock-Mass Quality Category 2 (Basecase 2)

Figure 4-16. Effects of drift excavation on yielding of rock (cont'd)

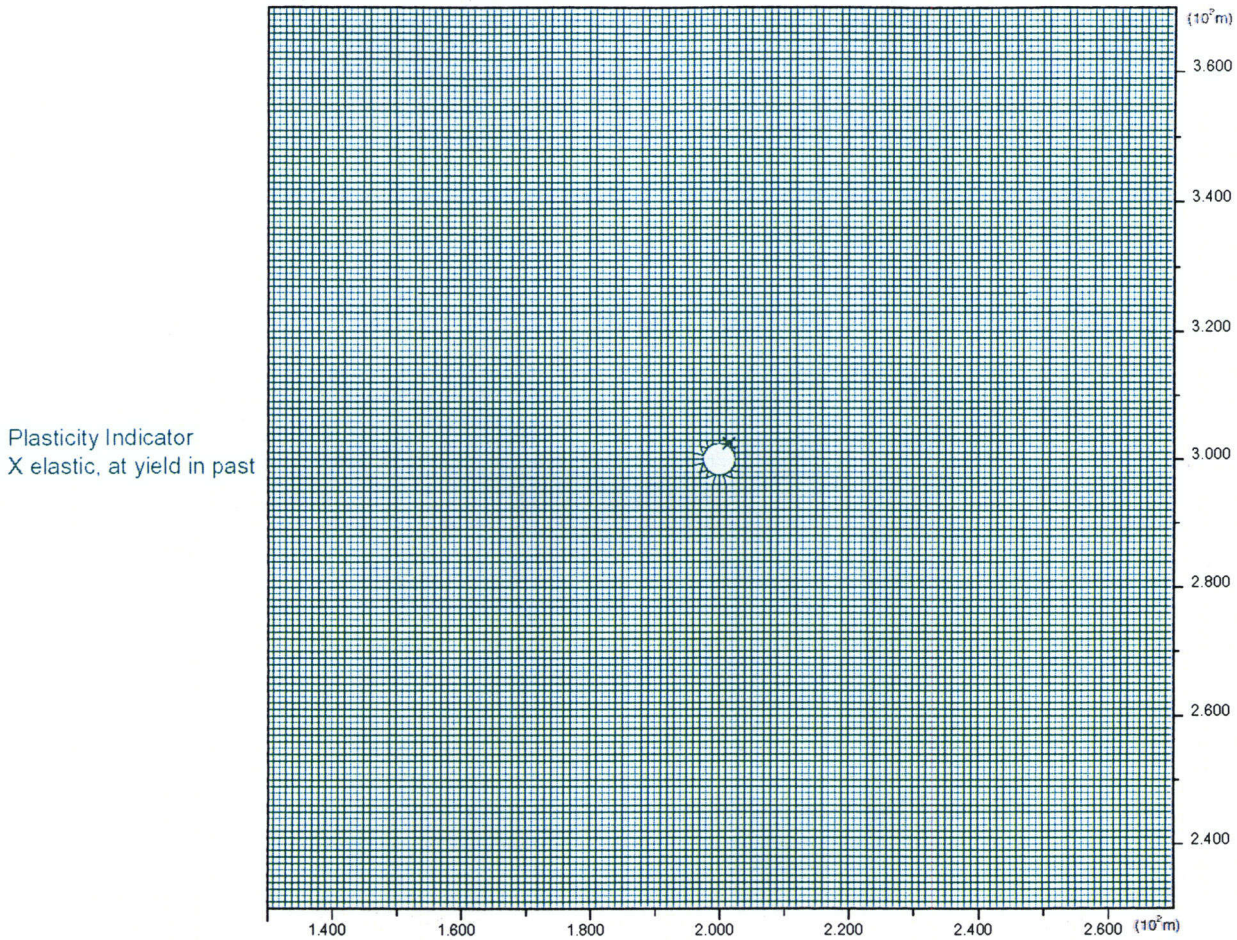

(c) Rock-Mass Quality Category 5 (Sensitivity Case 6)

Figure 4-16. Effects of drift excavation on yielding of rock (cont'd)

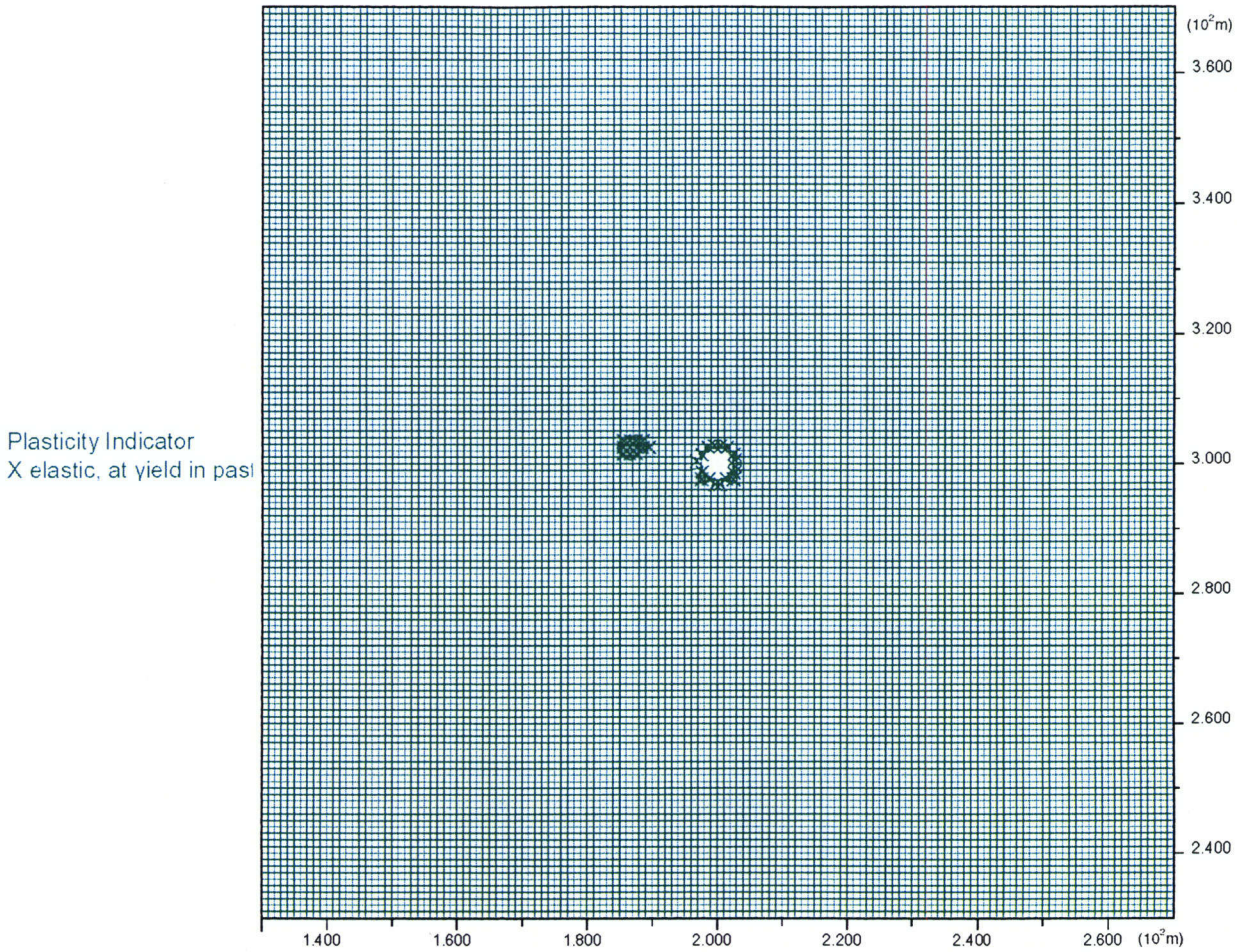

(a) After 3 Months of Heating

Figure 4-17. Extent of yielding in rock as a function of time for Sensitivity Case 5 with Temperature Option 1

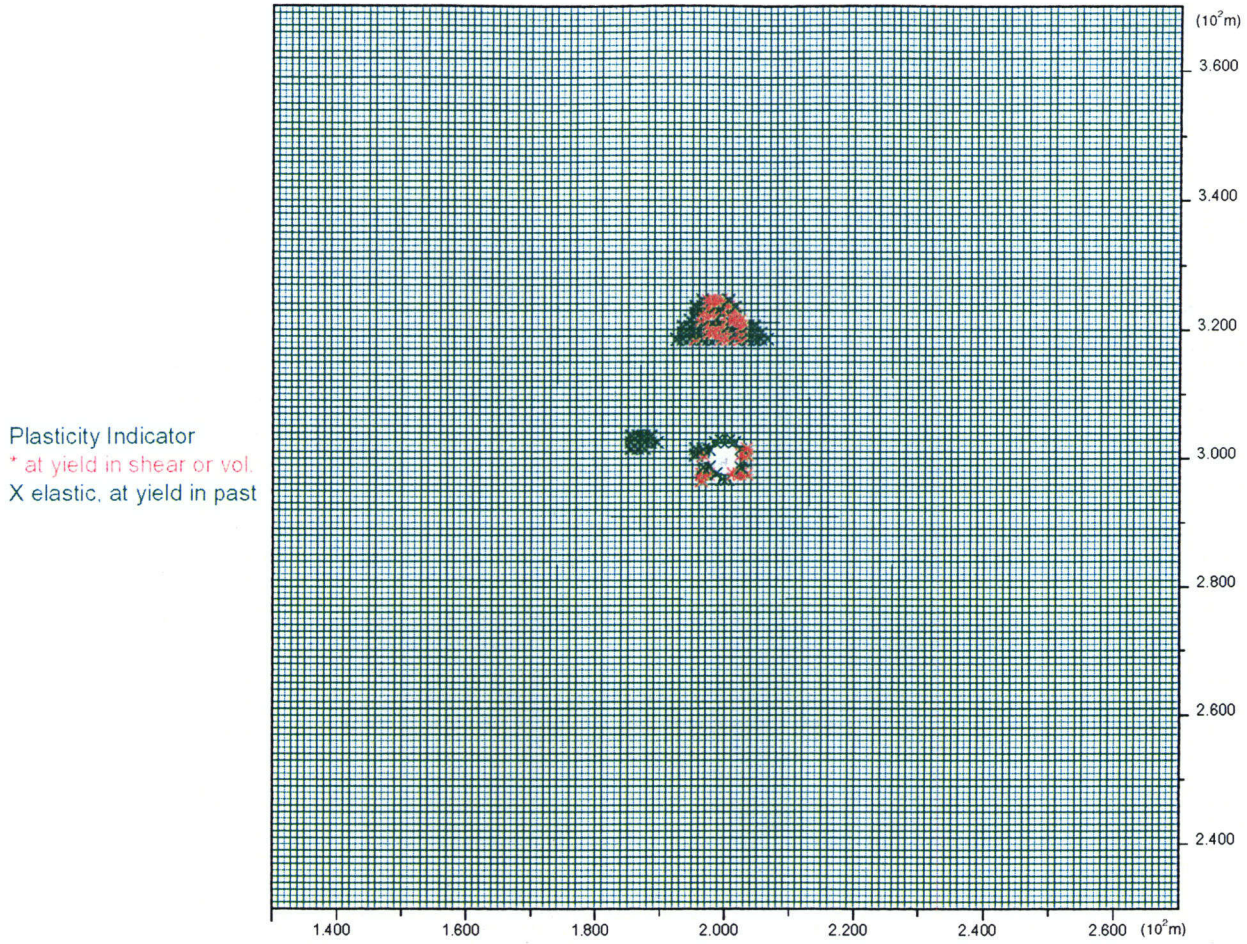

(b) After 1 Year of Heating

Figure 4-17. Extent of yielding in rock as a function of time for Sensitivity Case 5 with Temperature Option 1 (cont'd)

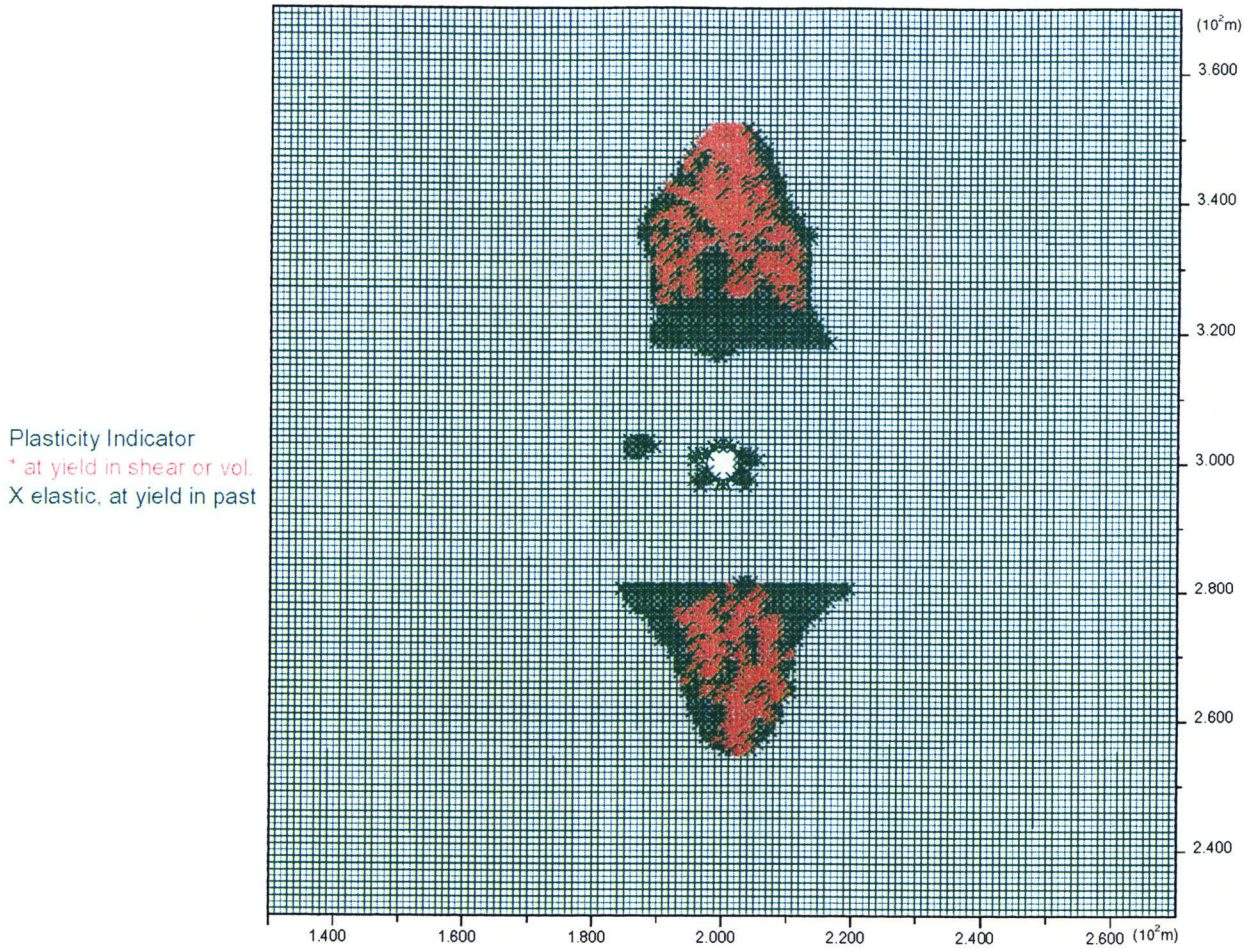

(c) After 4 Years of Heating

Figure 4-17. Extent of yielding in rock as a function of time for Sensitivity Case 5 with Temperature Option 1 (cont'd)

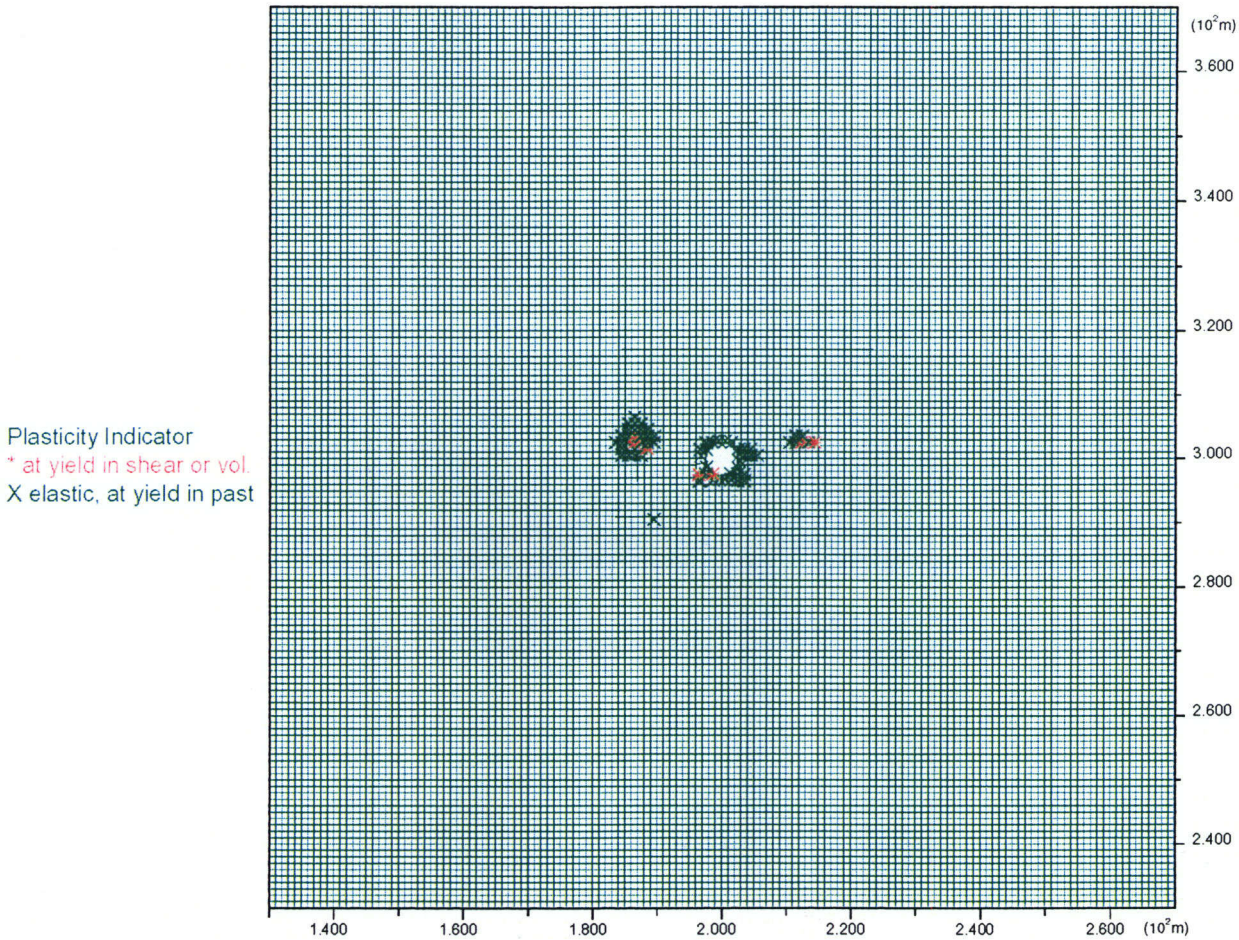

(a) After 3 Months of Heating

Figure 4-18. Extent of yielding in rock as a function of time for Basecase 2 with Temperature Option 1

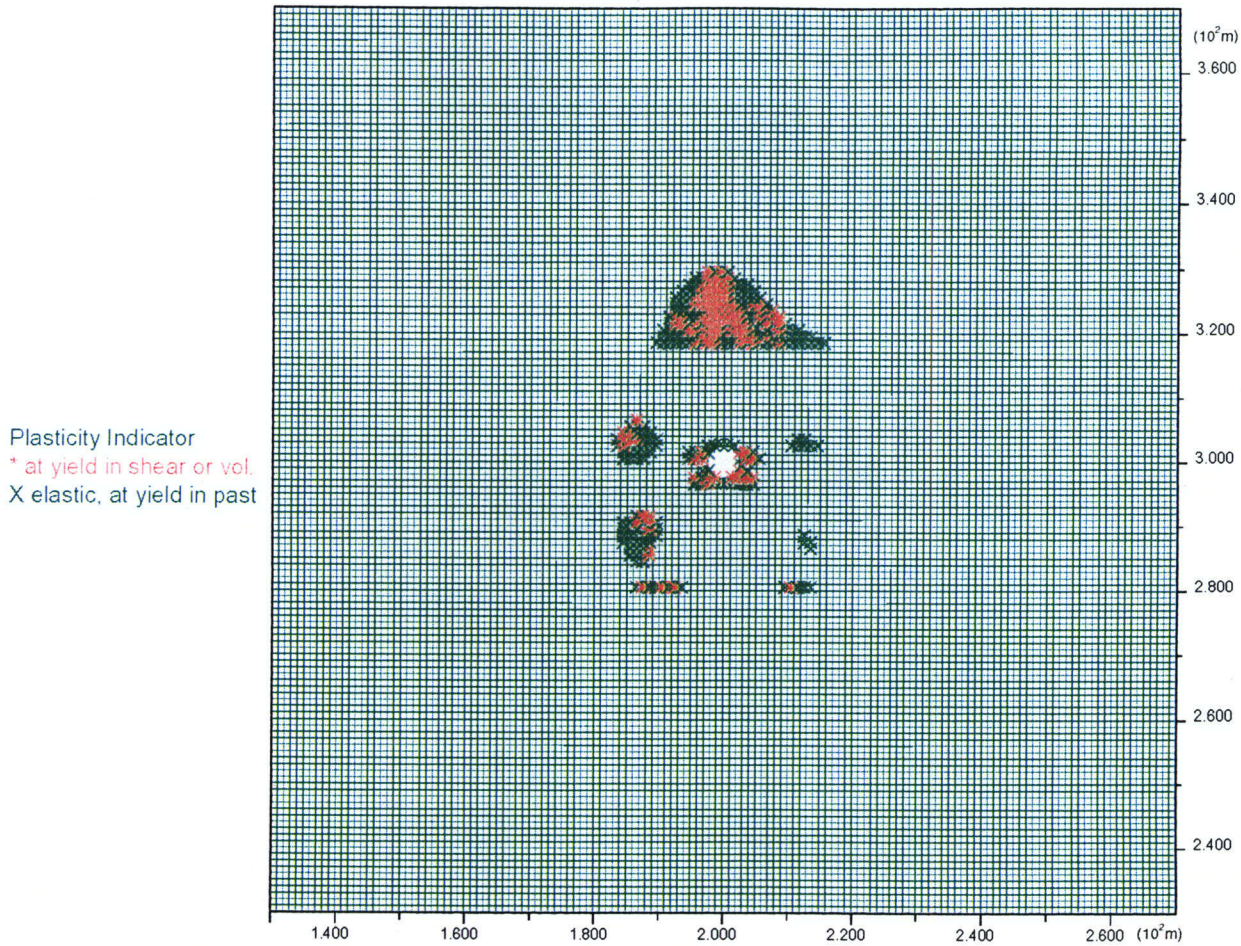

(b) After 1 Year of Heating

Figure 4-18. Extent of yielding in rock as a function of time for Basecase 2 with Temperature Option 1 (cont'd)

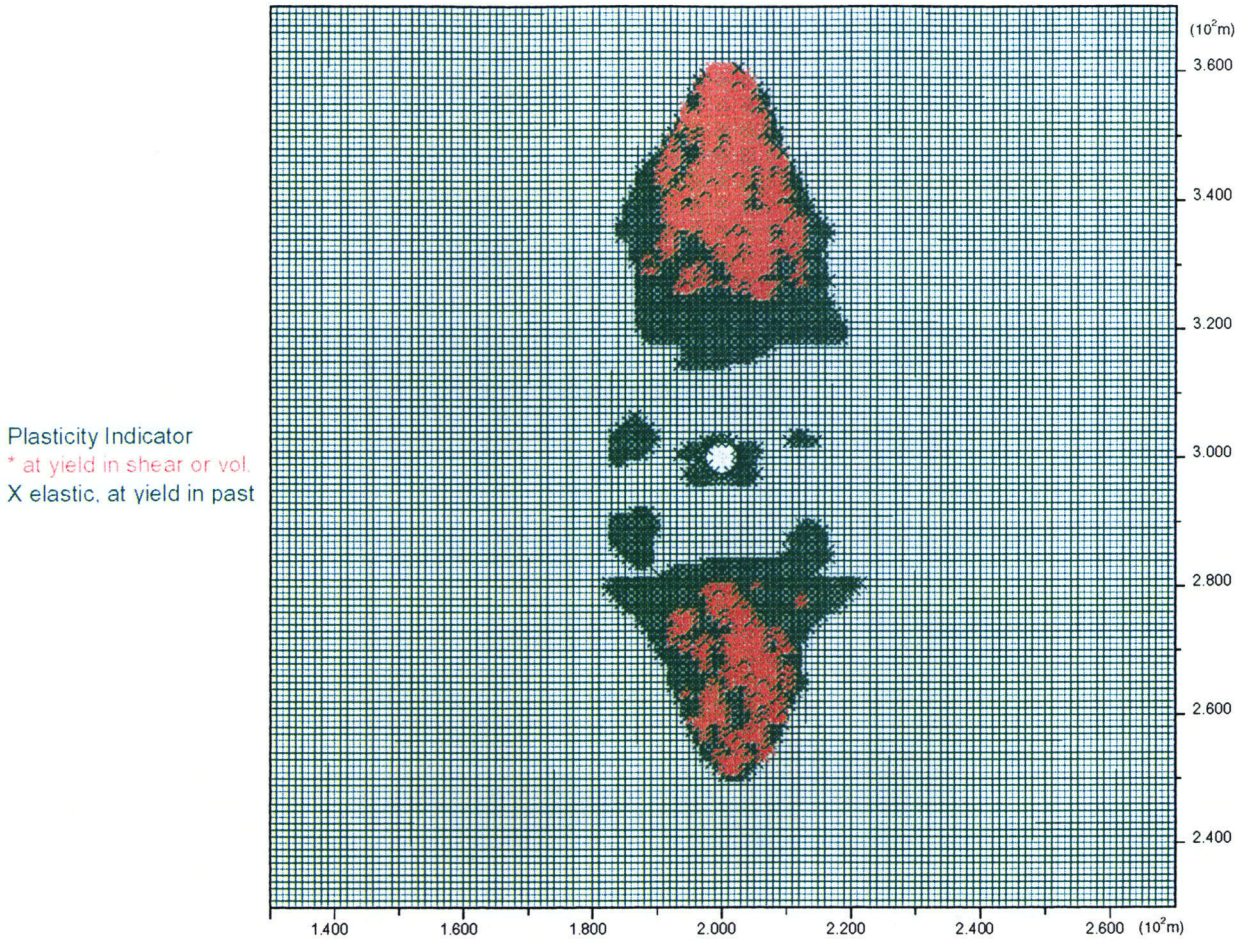

(c) After 4 Years of Heating

Figure 4-18. Extent of yielding in rock as a function of time for Basecase 2 with Temperature Option 1 (cont'd)

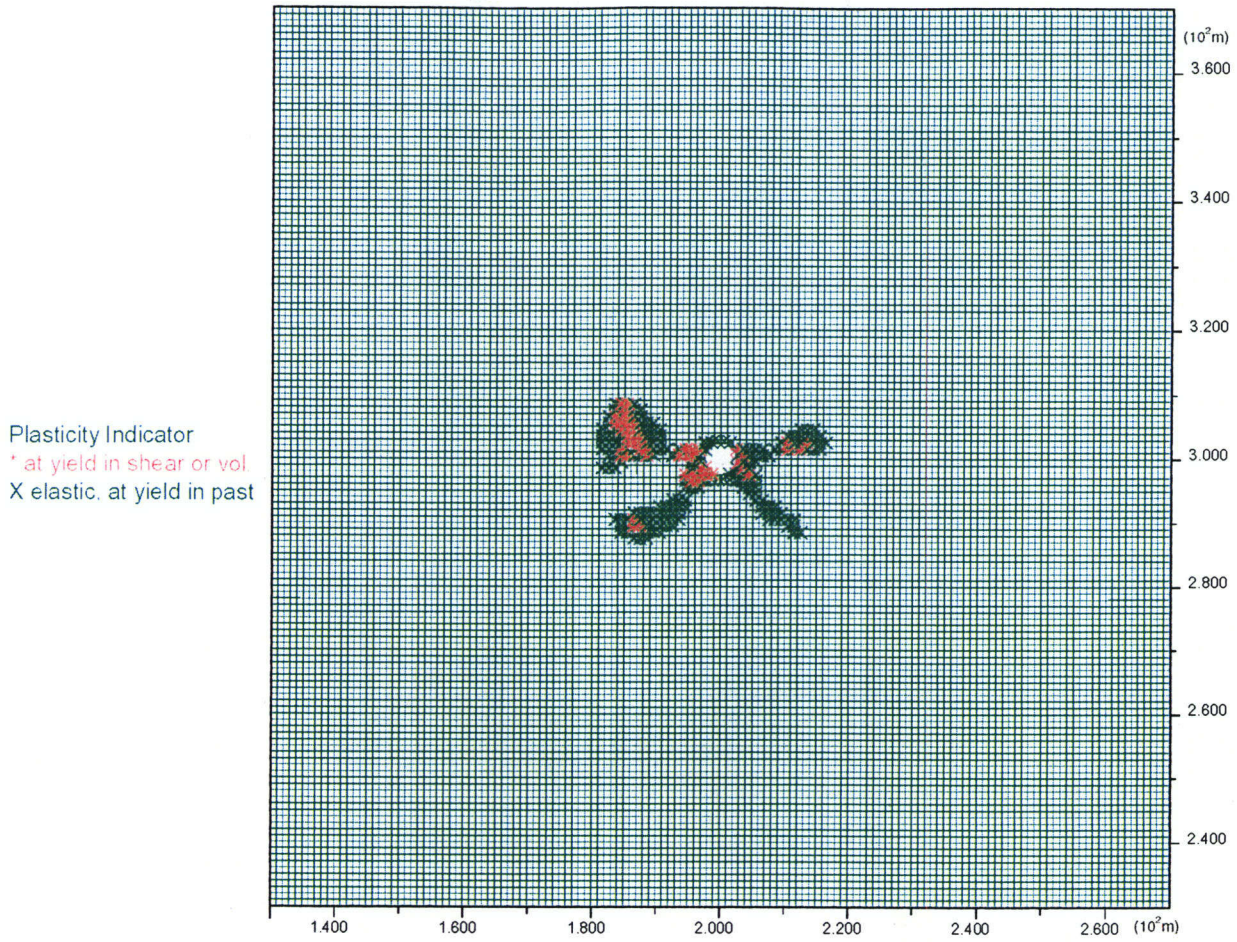

(a) After 3 Months of Heating

Figure 4-19. Extent of yielding in rock as a function of time for Sensitivity Case 6 with Temperature Option 1

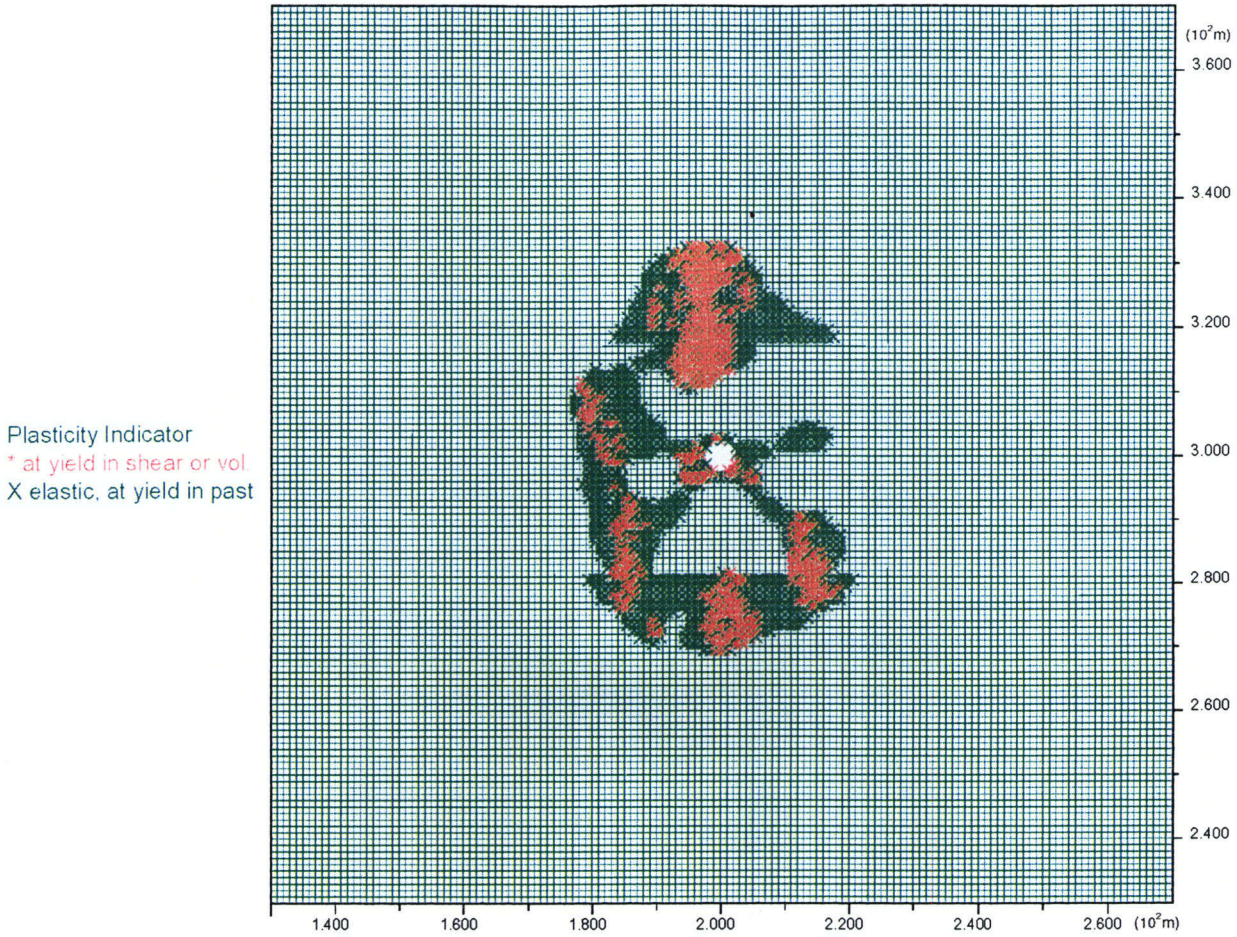

(b) After 1 Year of Heating

Figure 4-19. Extent of yielding in rock as a function of time for Sensitivity Case 6 with Temperature Option 1 (cont'd)

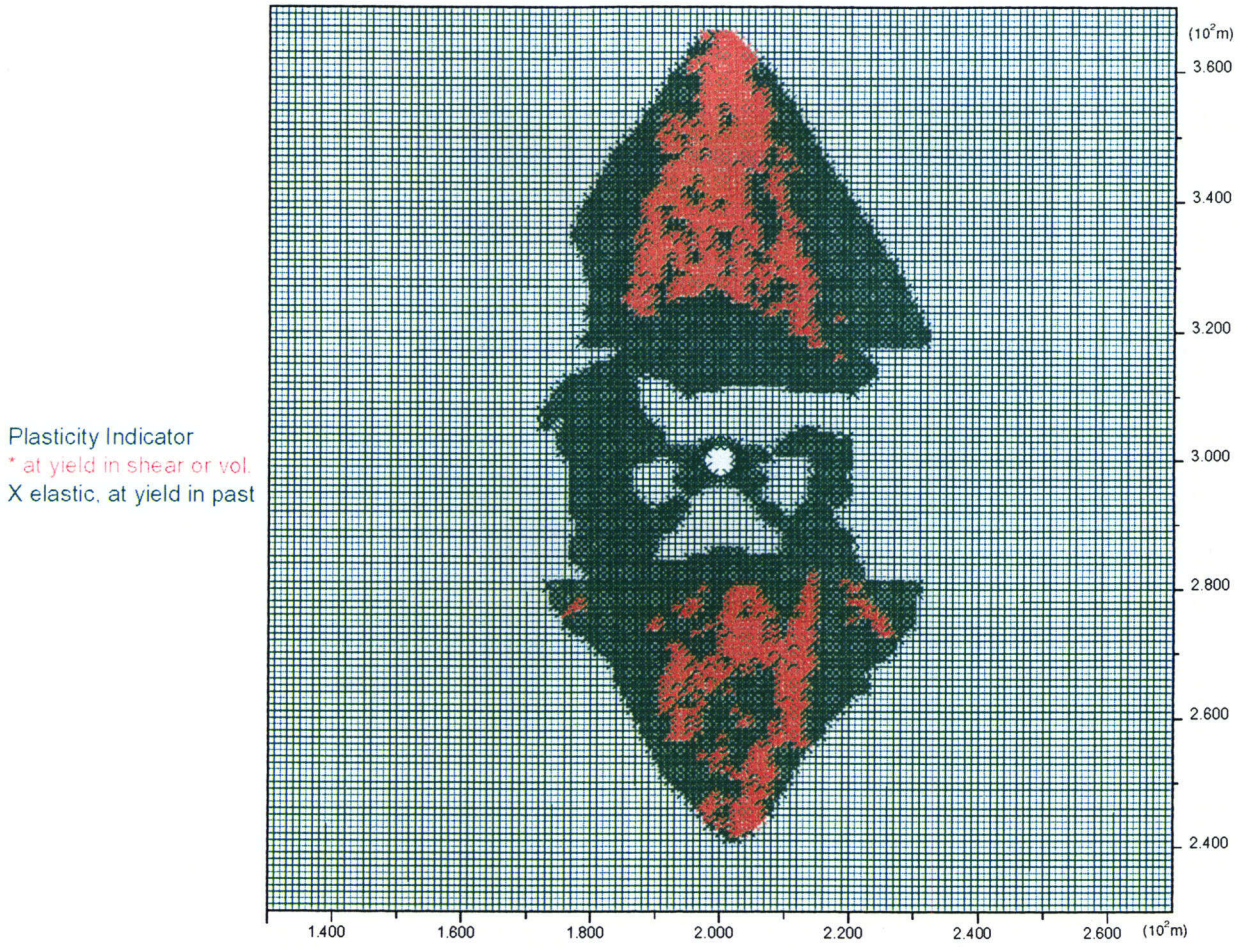

(c) After 4 Years of Heating

Figure 4-19. Extent of yielding in rock as a function of time for Sensitivity Case 6 with Temperature Option 1 (cont'd)

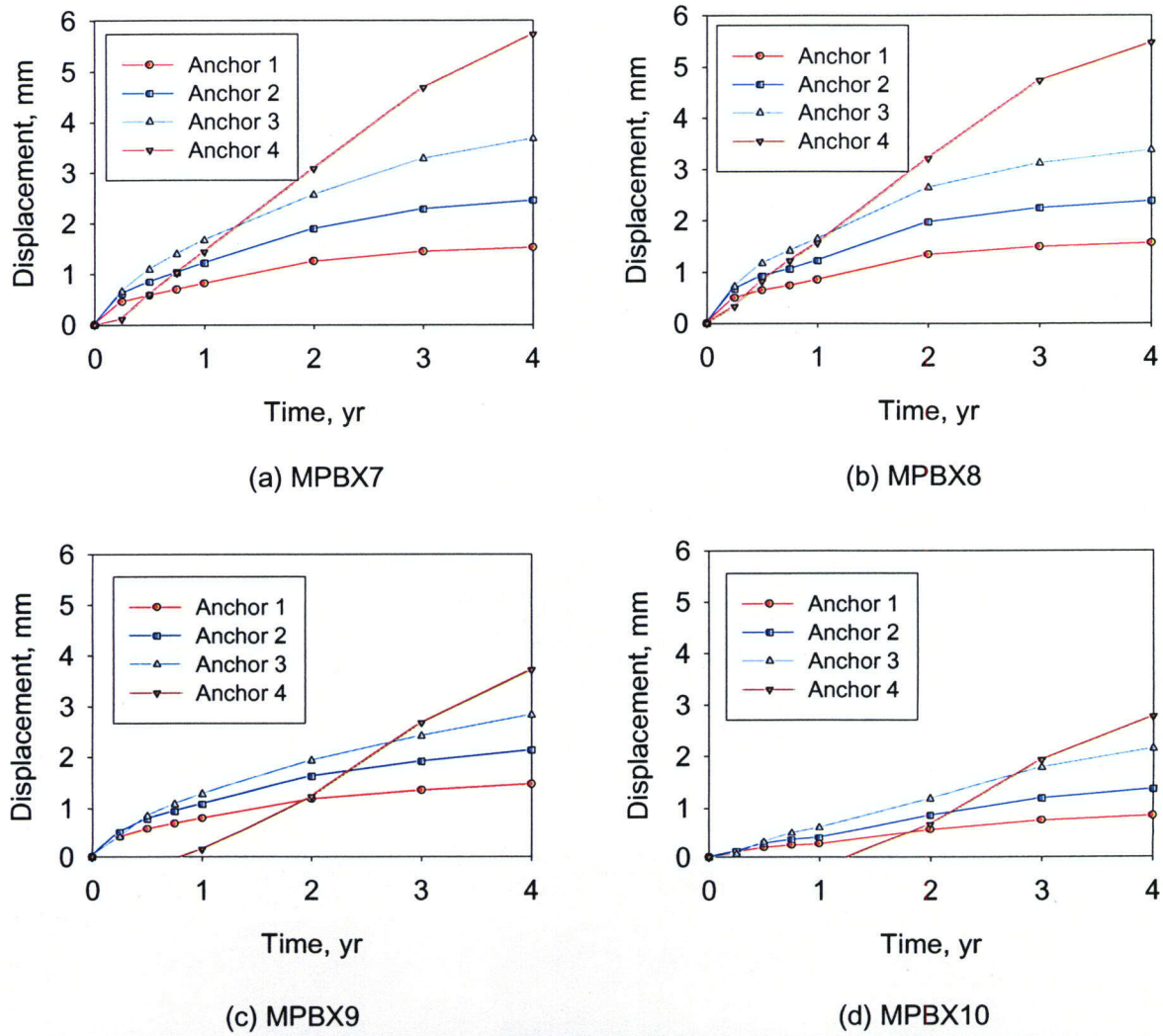

Figure 4-20. Predicted anchor displacements for Basecase 1 with Temperature Option 1

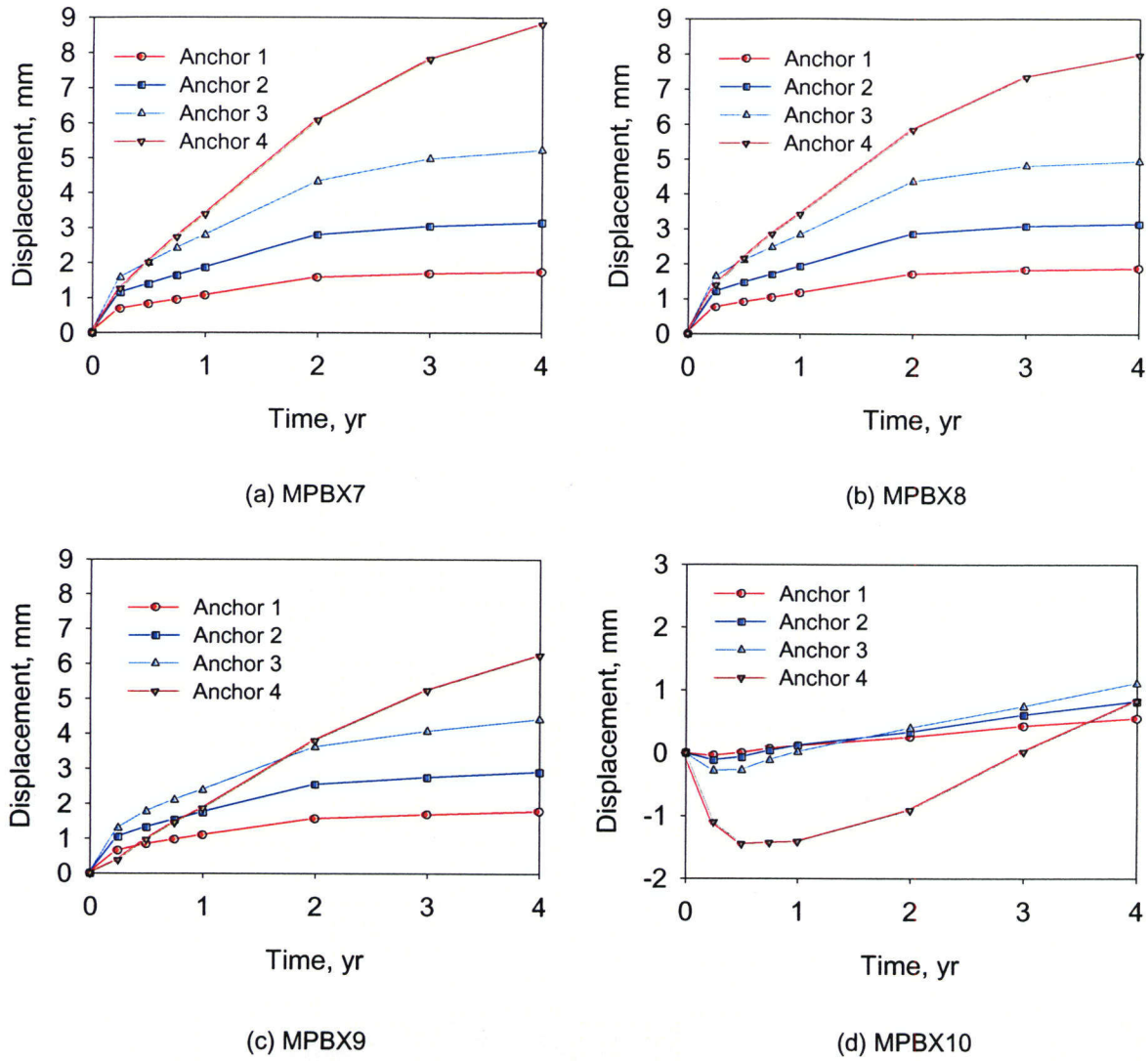

Figure 4-21. Predicted anchor displacements for Basecase 1 with Temperature Option 2

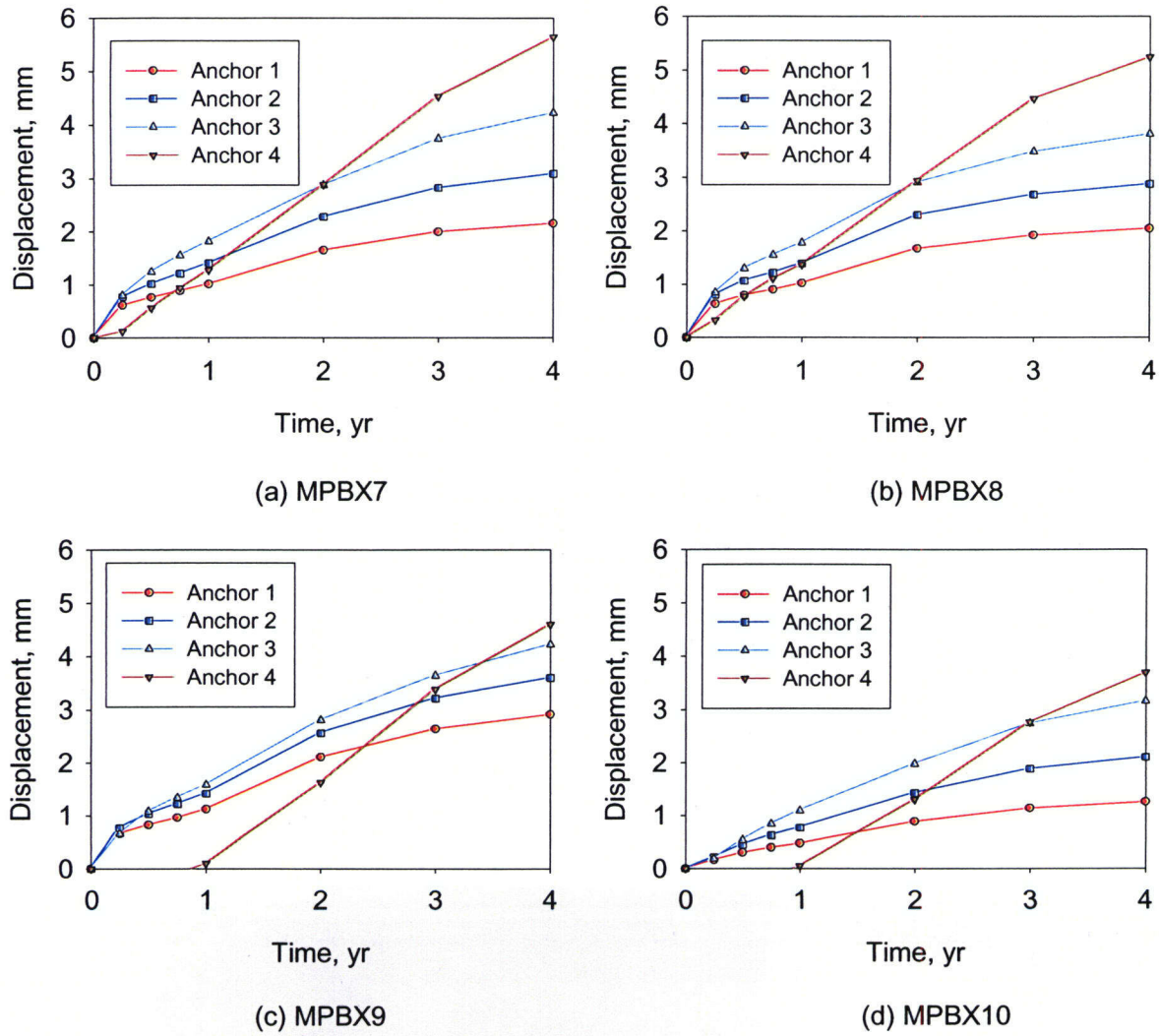

Figure 4-22. Predicted anchor displacements for Basecase 2 with Temperature Option 1

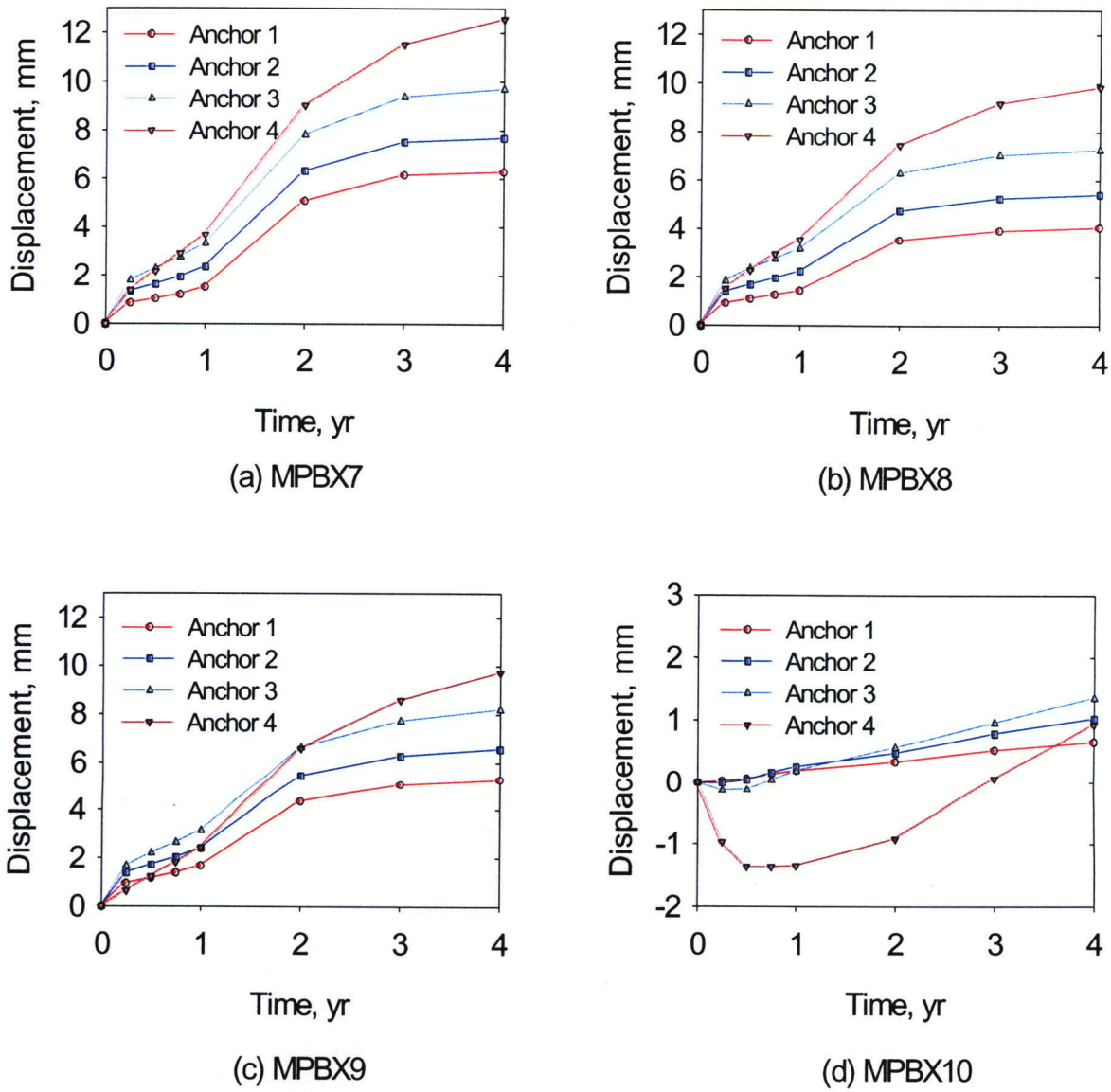

Figure 4-23. Predicted anchor displacements for Basecase 2 with Temperature Option 2

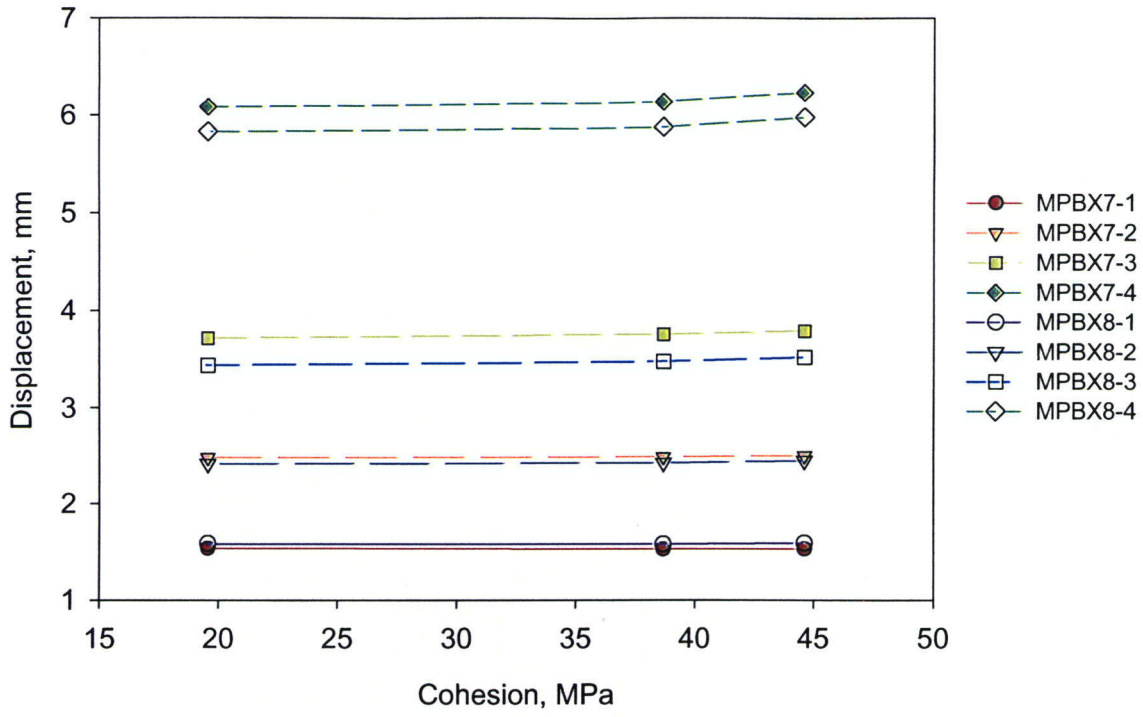

Figure 4-24. Effects of cohesion on rock deformation, Temperature Option 1

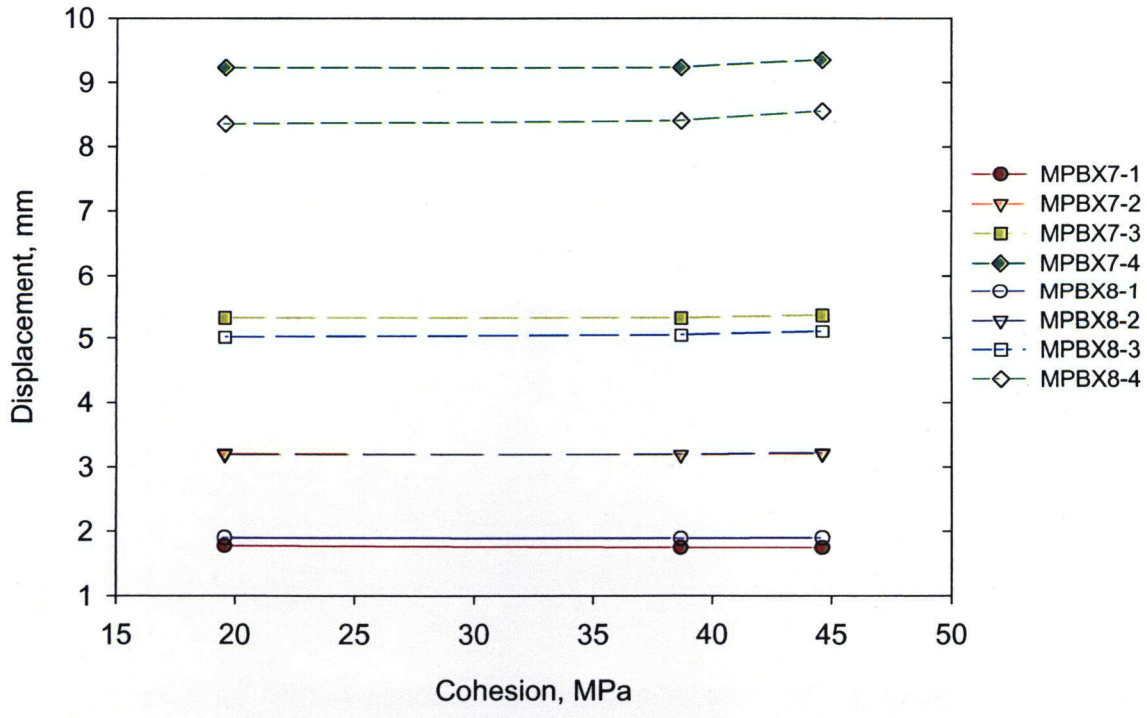

Figure 4-25. Effects of cohesion on rock deformation, Temperature Option 2

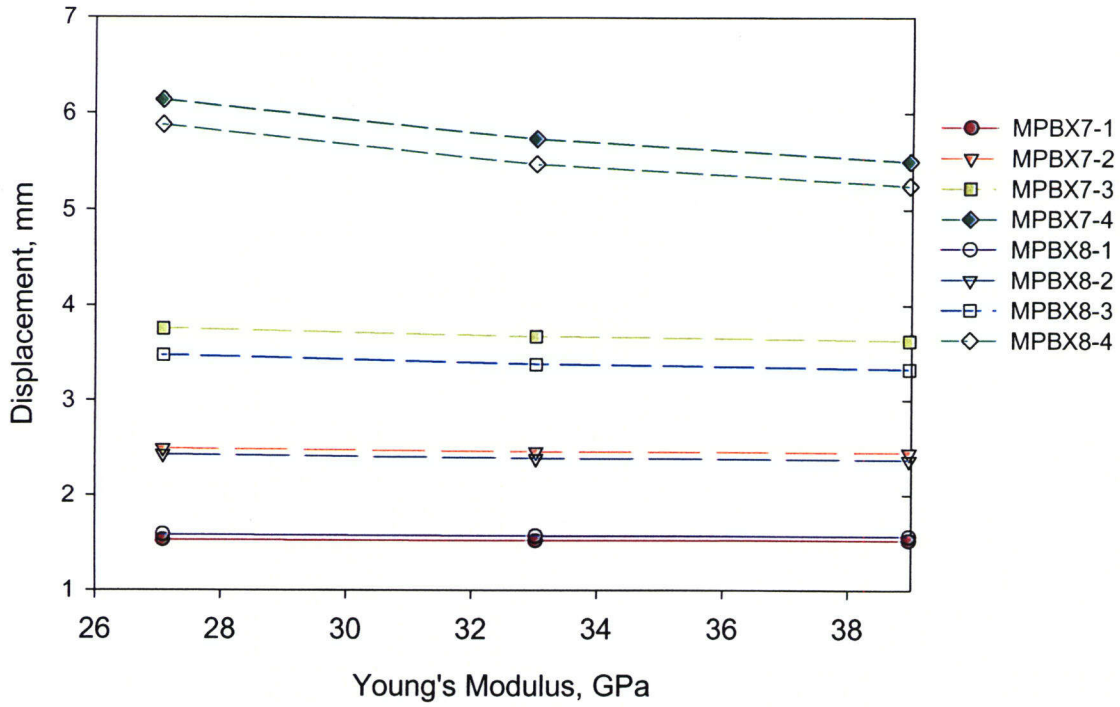

Figure 4-26. Effect of Young's modulus on displacements of anchors in rock, Temperature Option 1

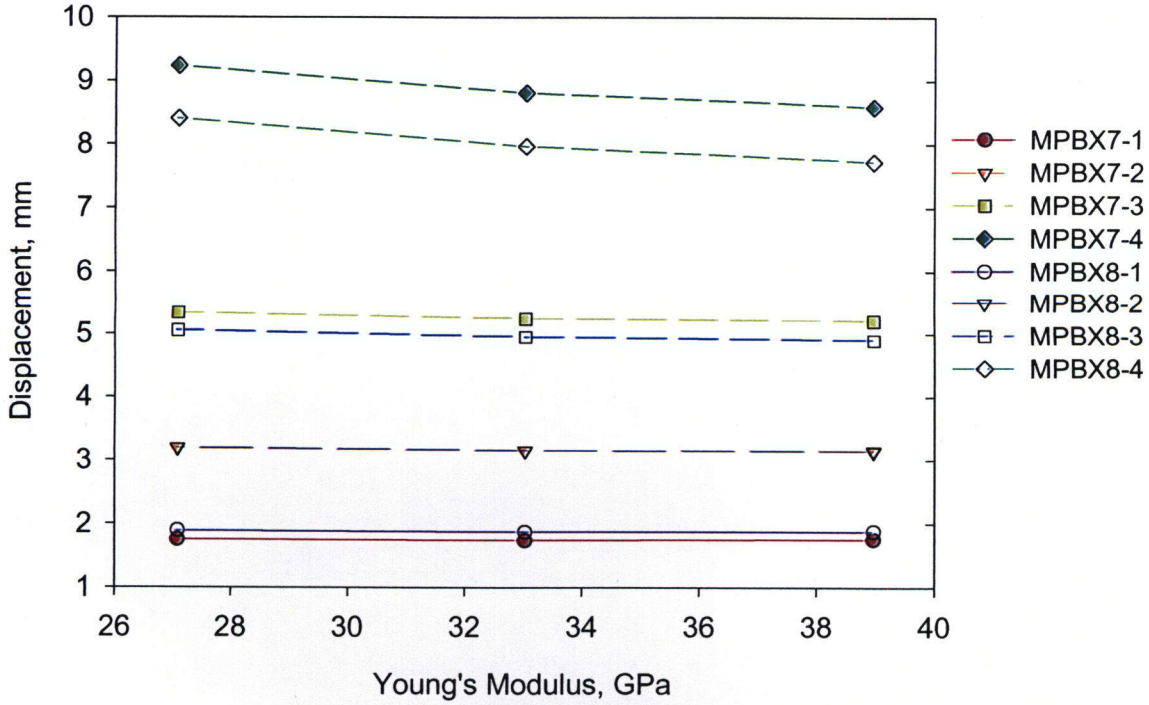

Figure 4-27. Effect of Young's modulus on displacements of anchors in rock, Temperature Option 2

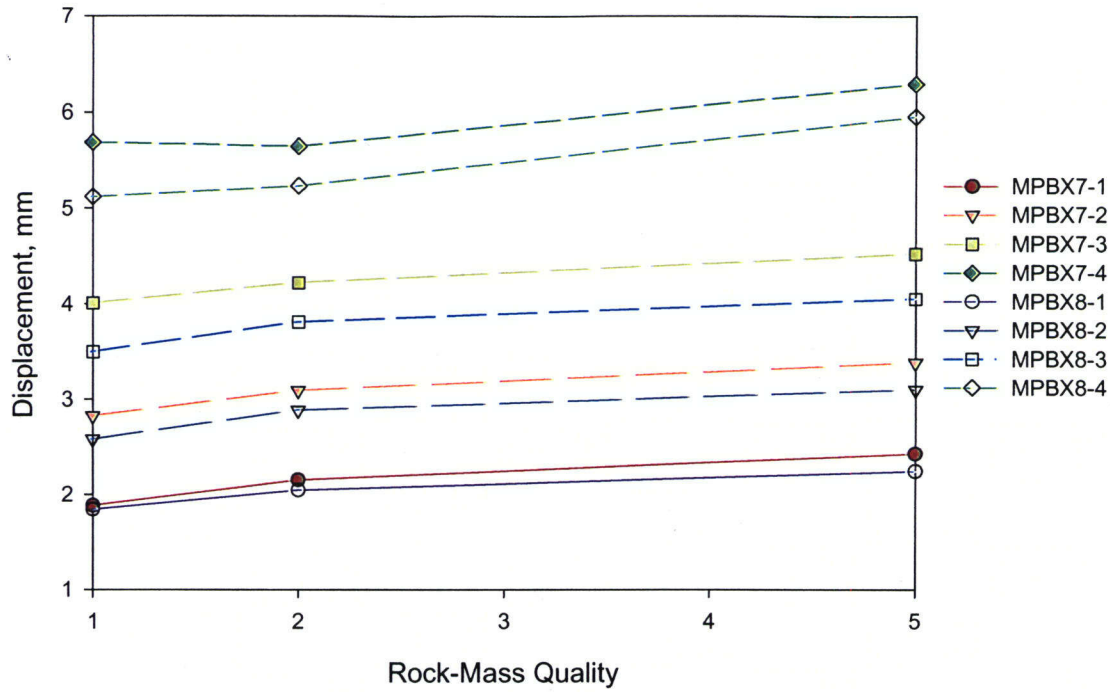

Figure 4-28. Anchor displacements as a function of rock-mass quality, Temperature Option 1

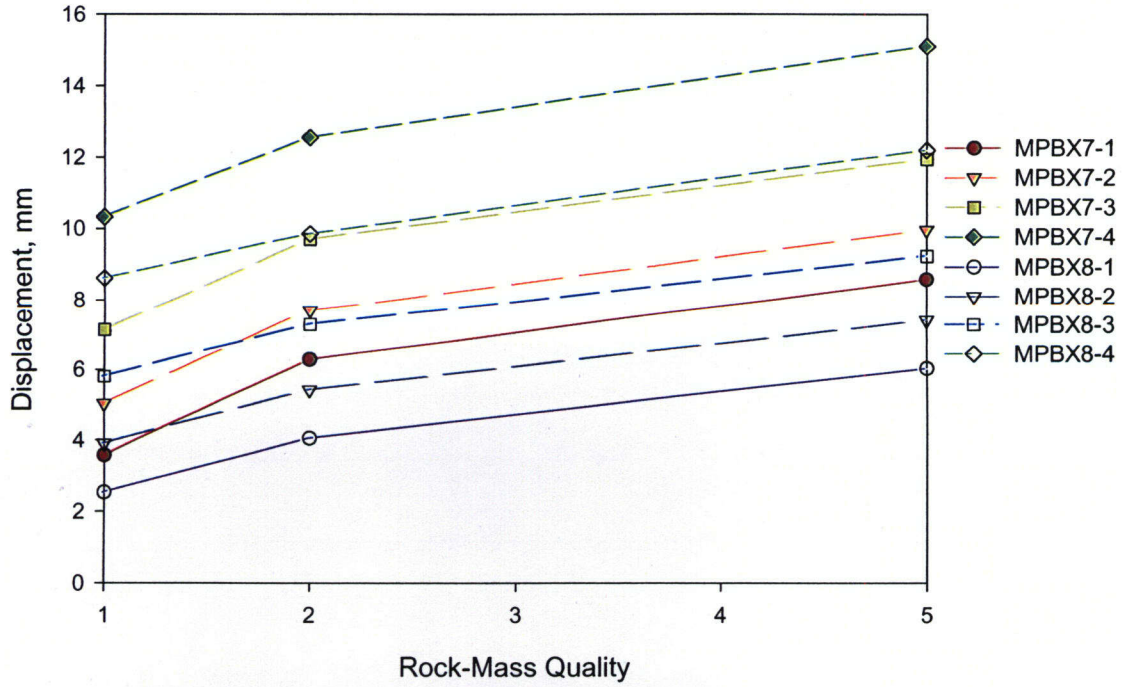

Figure 4-29. Anchor displacements as a function of rock-mass quality, Temperature Option 2

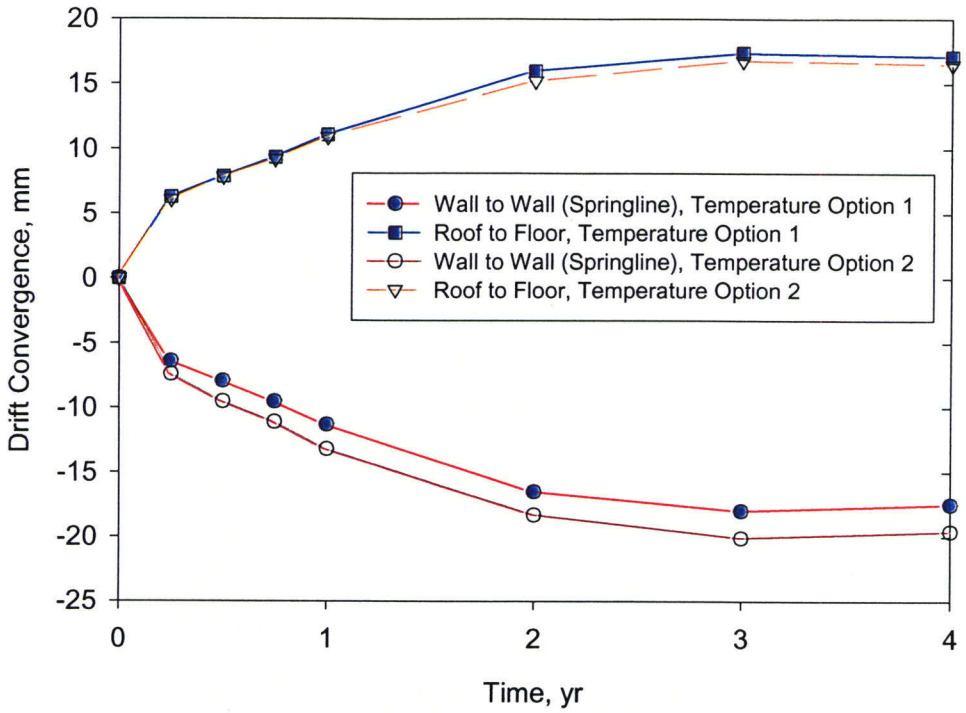

Figure 4-30. Drift convergence for Basecase 1

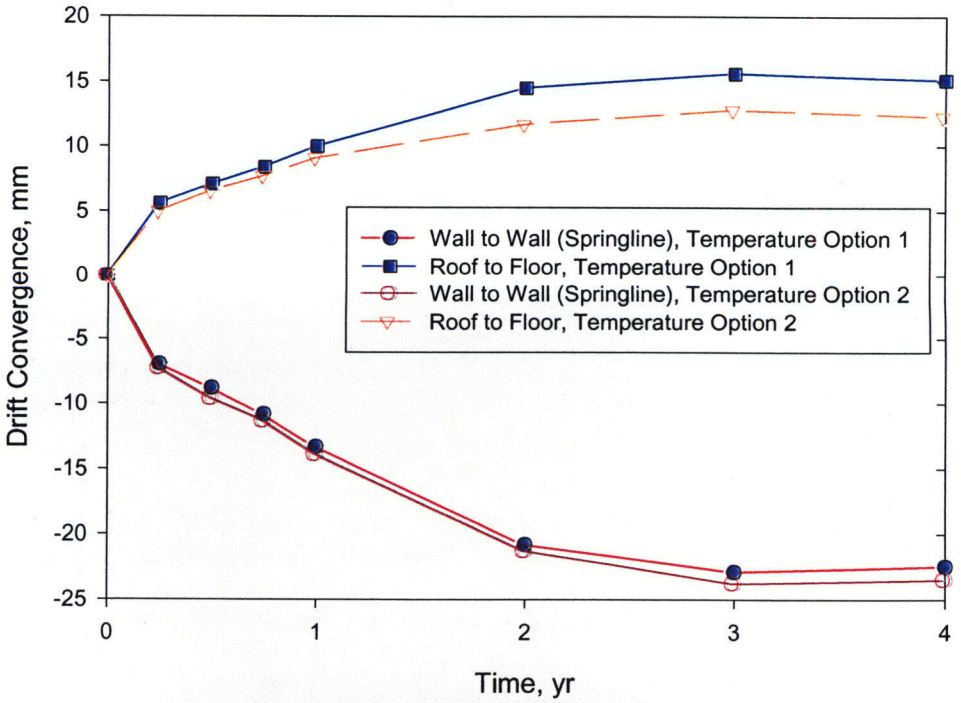

Figure 4-31. Drift convergence for Basecase 2

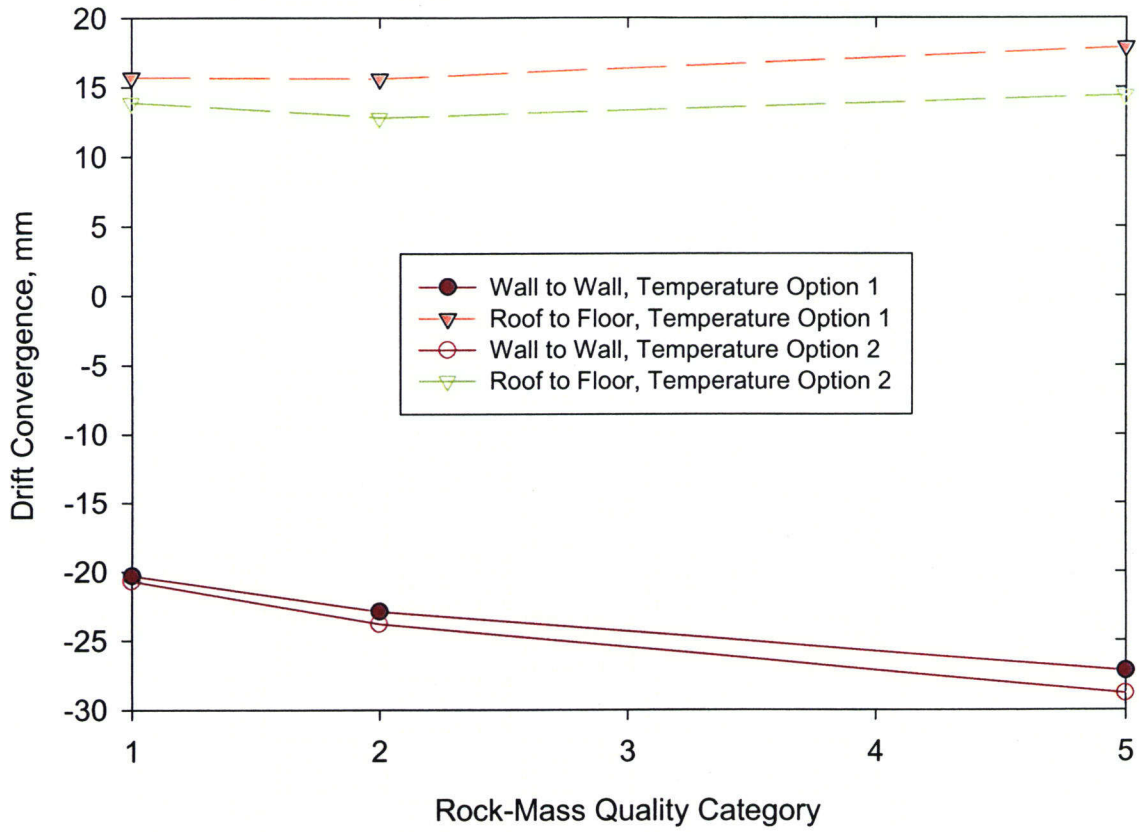

Figure 4-32. Drift convergence as a function of rock-mass quality after 3 years of heating

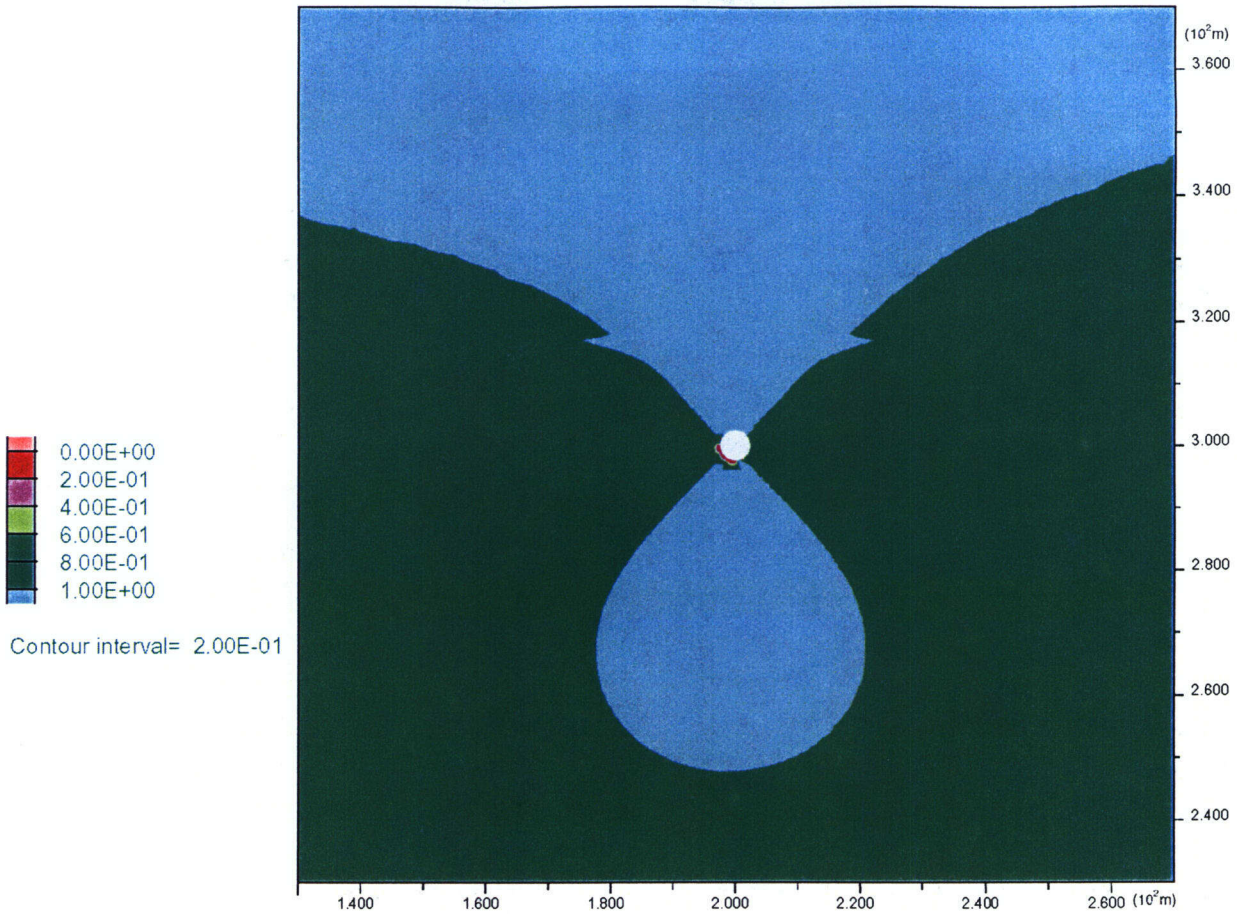

Figure 4-33. Effect of drift excavation on permeability for Basecase 1

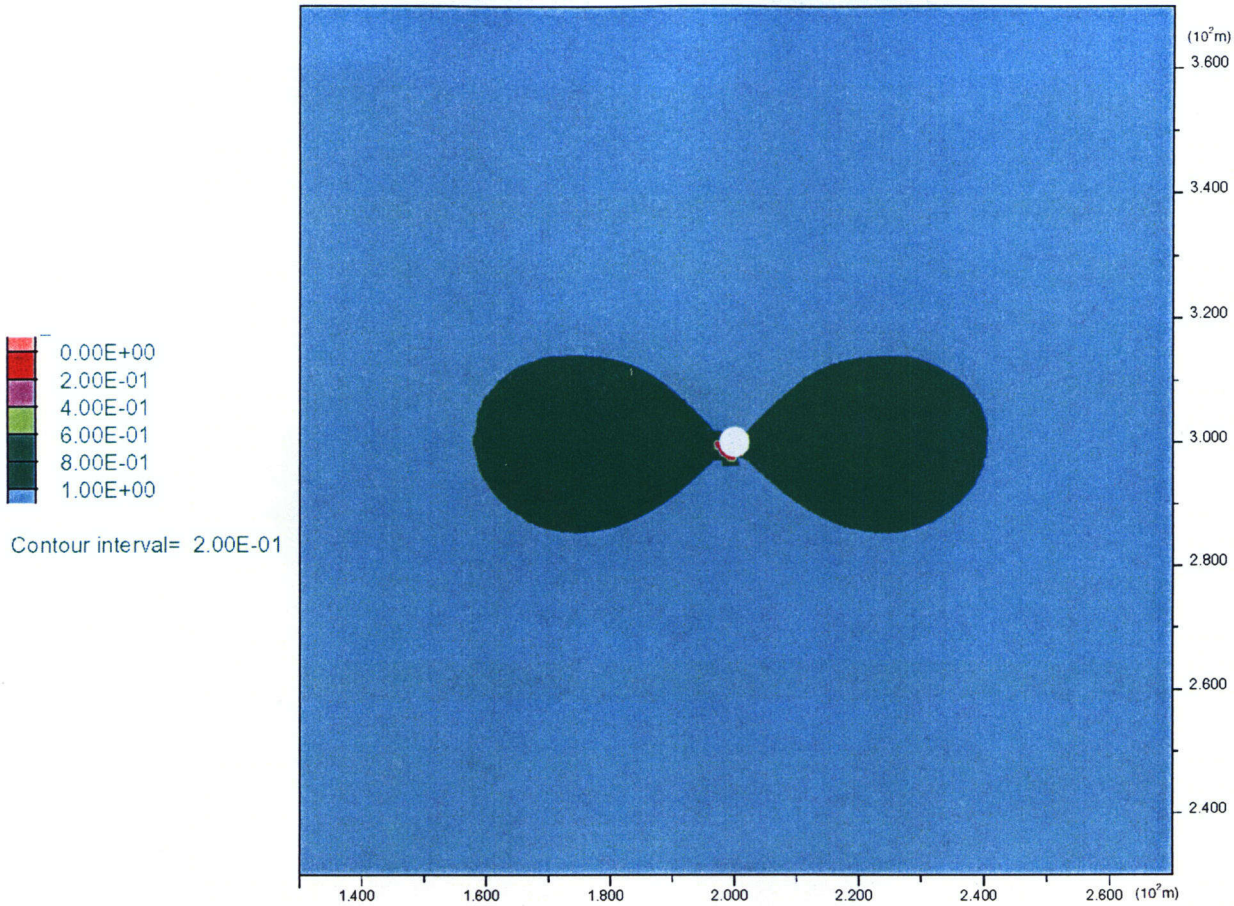

Figure 4-34. Effect of drift excavation on permeability for Sensitivity Case 2

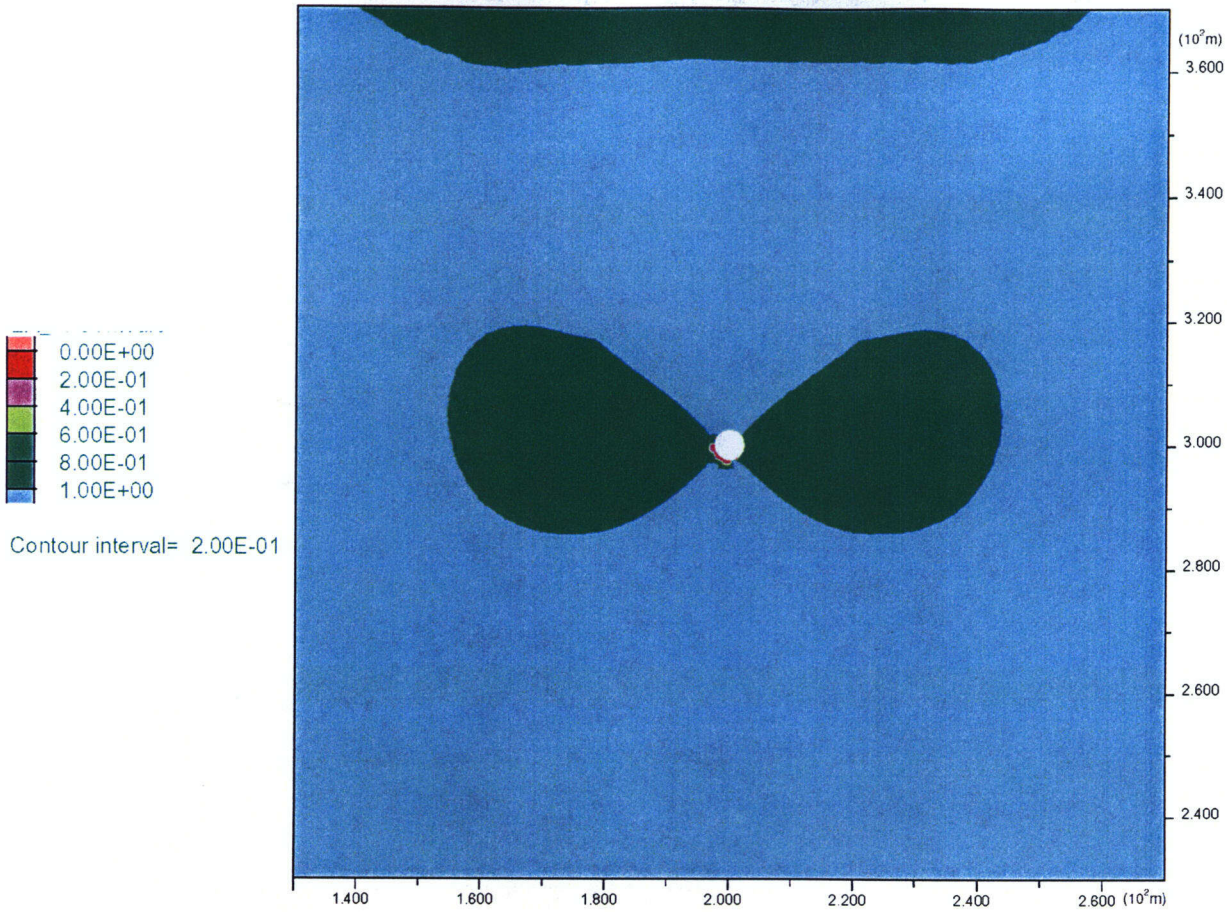

Figure 4-35. Effect of drift excavation on permeability for Basecase 2

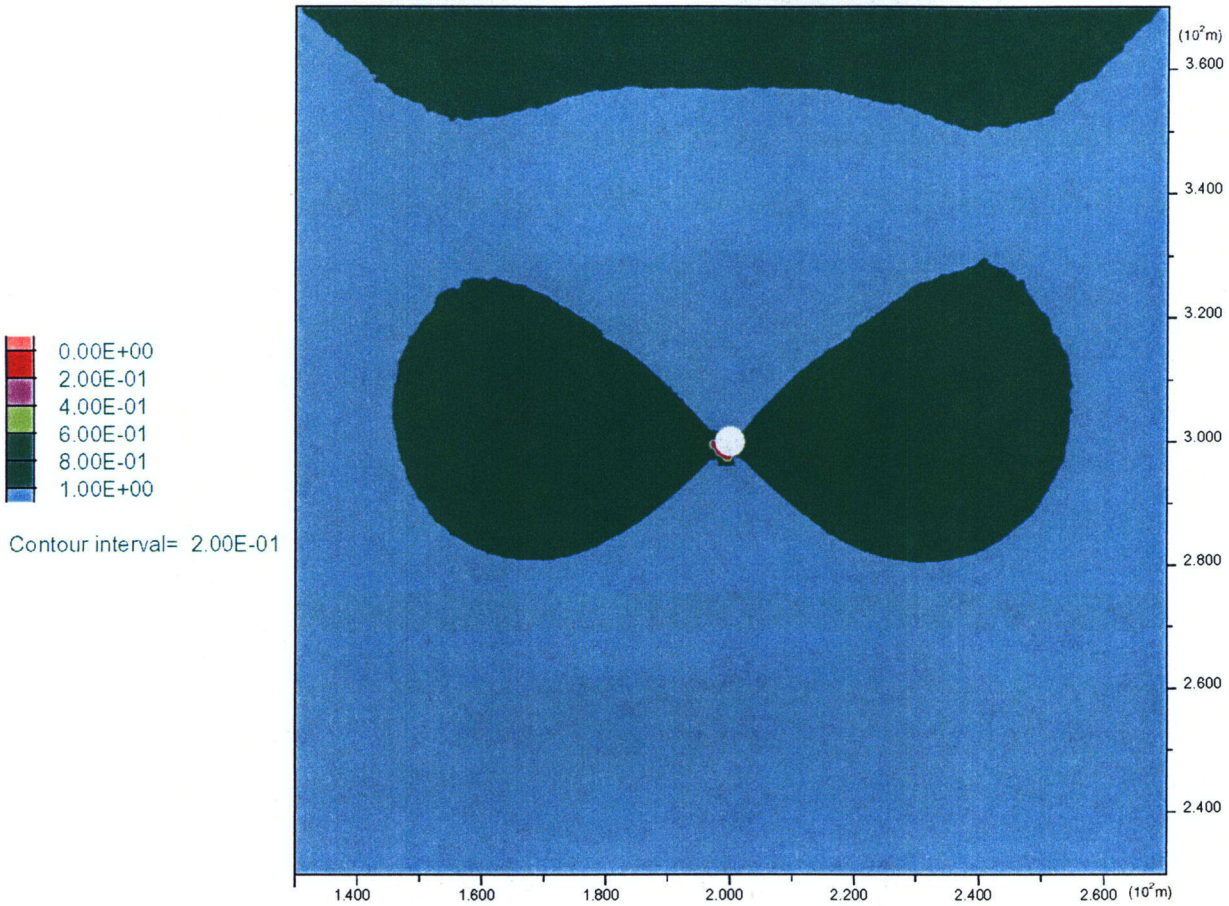

Figure 4-36. Effect of drift excavation on permeability for Sensitivity Case 6

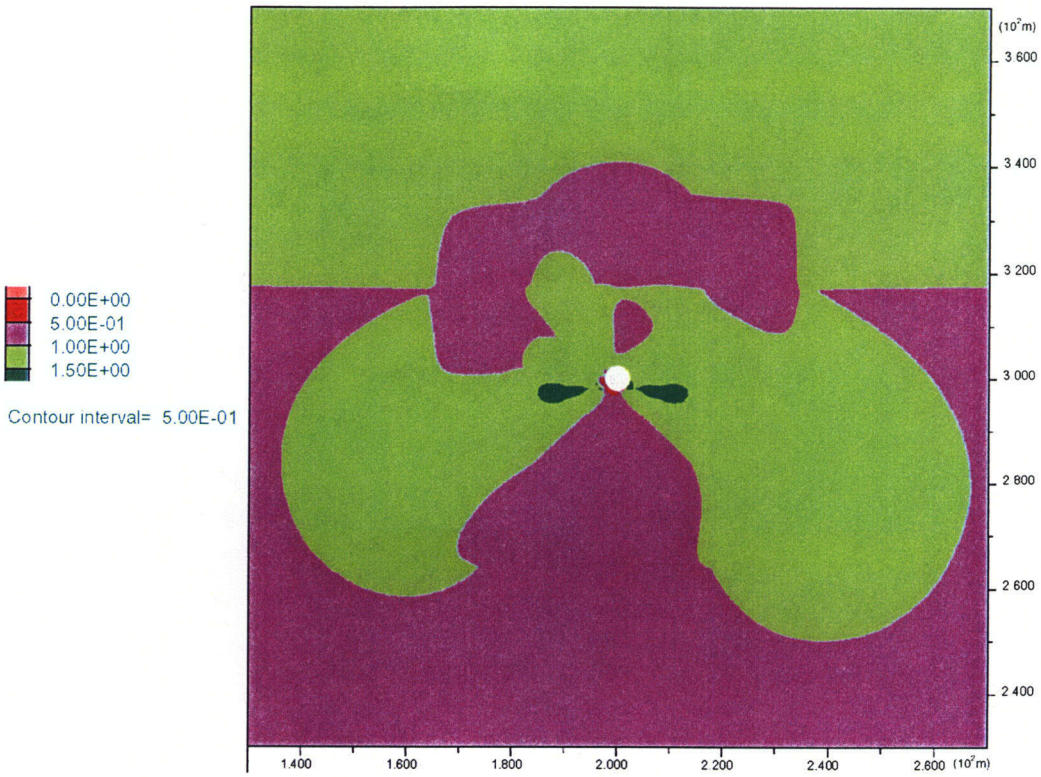

(a) After 3 Months of Heating

Figure 4-37. Permeability variation due to thermally induced deformation for Basecase 1 with Temperature Option 1

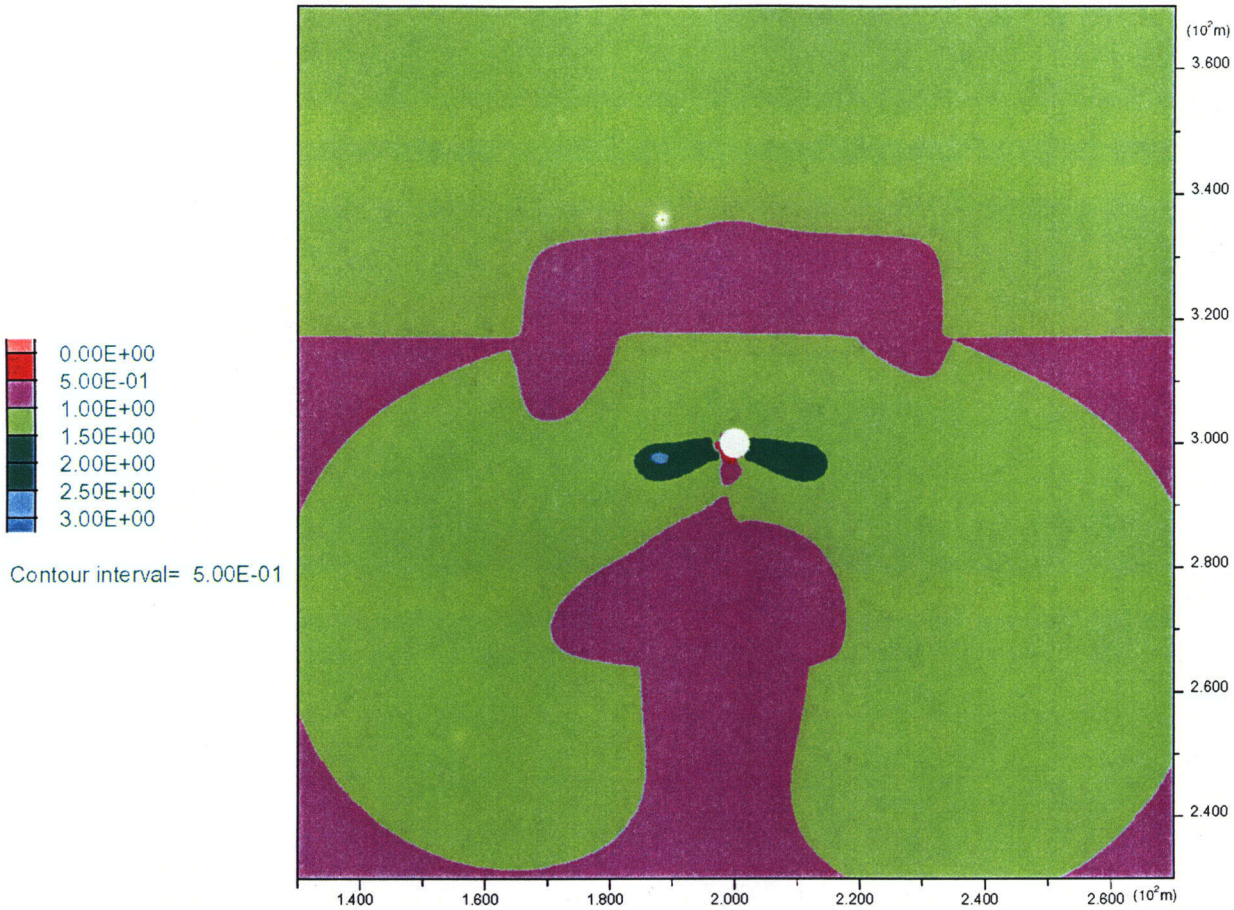

(b) After 1 Year of Heating

Figure 4-37. Permeability variation due to thermally induced deformation for Basecase 1 with Temperature Option 1 (cont'd)

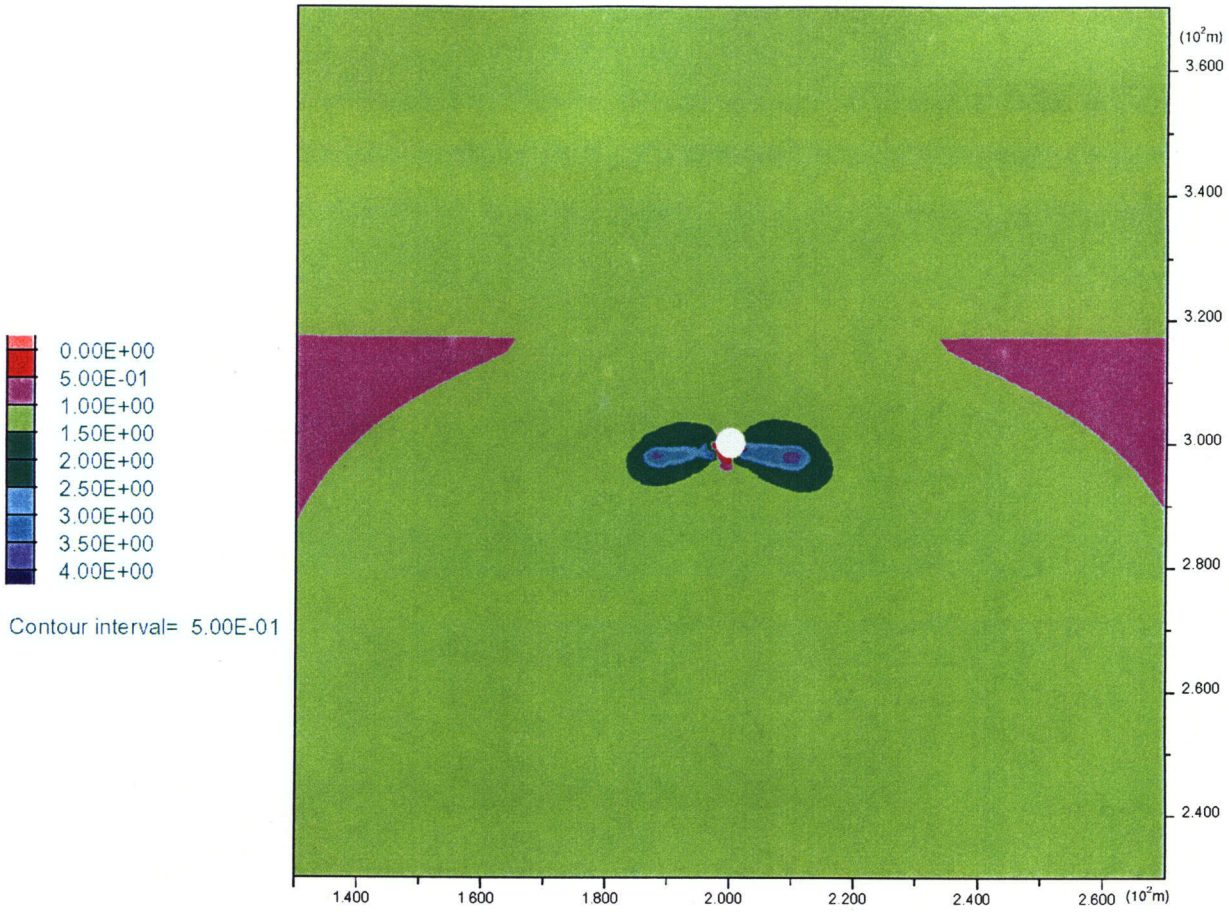

(c) After 4 Years of Heating

Figure 4-37. Permeability variation due to thermally induced deformation for Basecase 1 with Temperature Option 1 (cont'd)

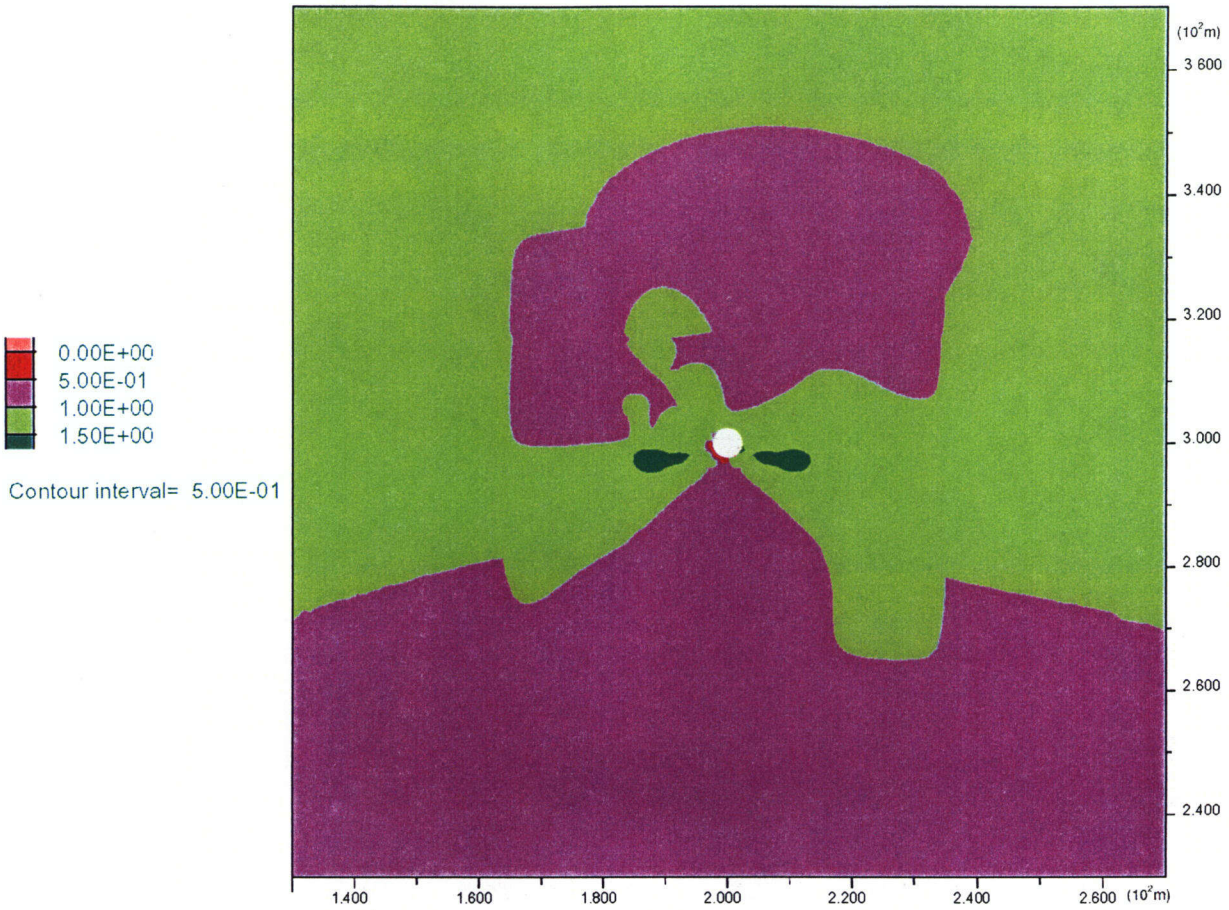

(a) After 3 Months of Heating

Figure 4-38. Permeability variation due to thermally induced deformation for Basecase 2 with Temperature Option 1

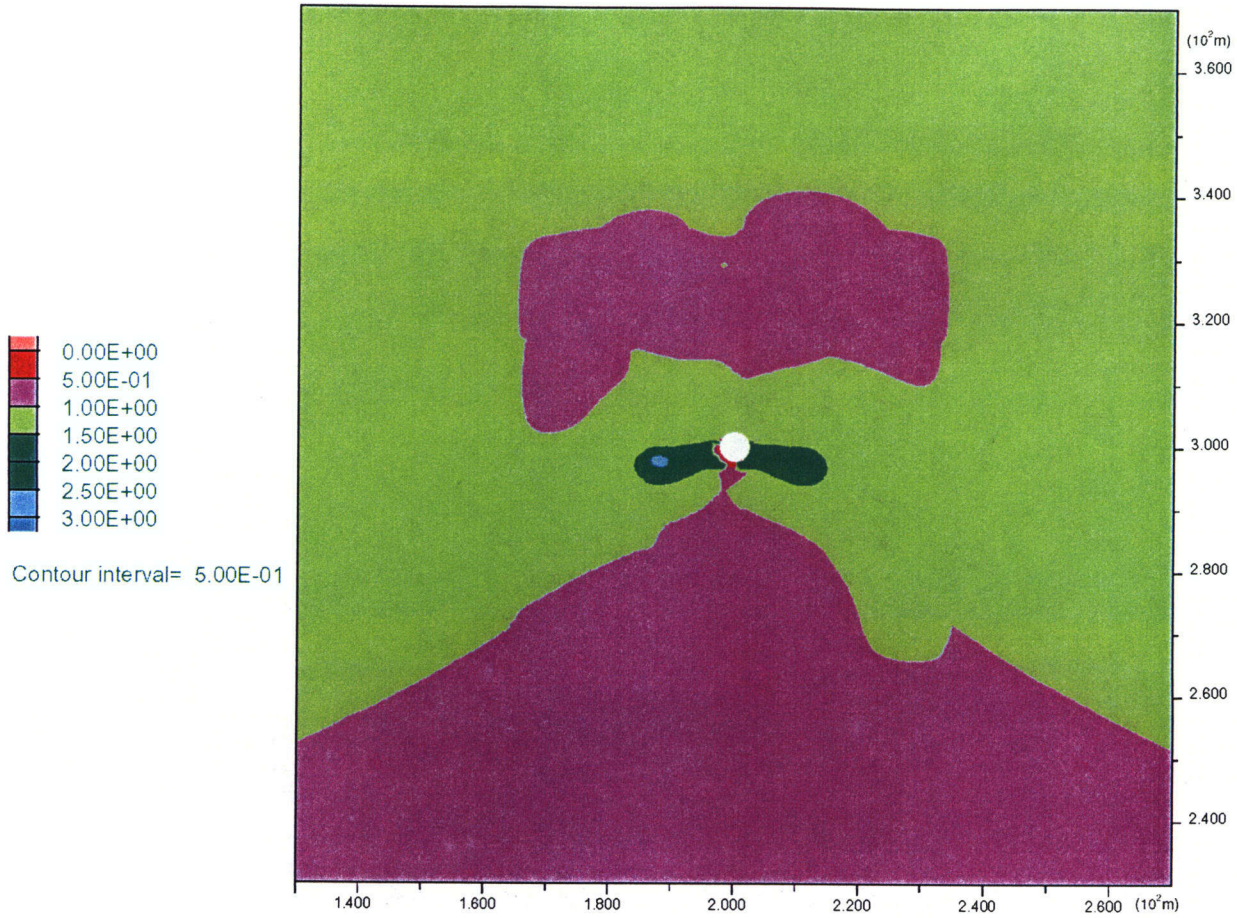

(b) After 1 Year of Heating

Figure 4-38. Permeability variation due to thermally induced deformation for Basecase 2 with Temperature Option 1 (cont'd)

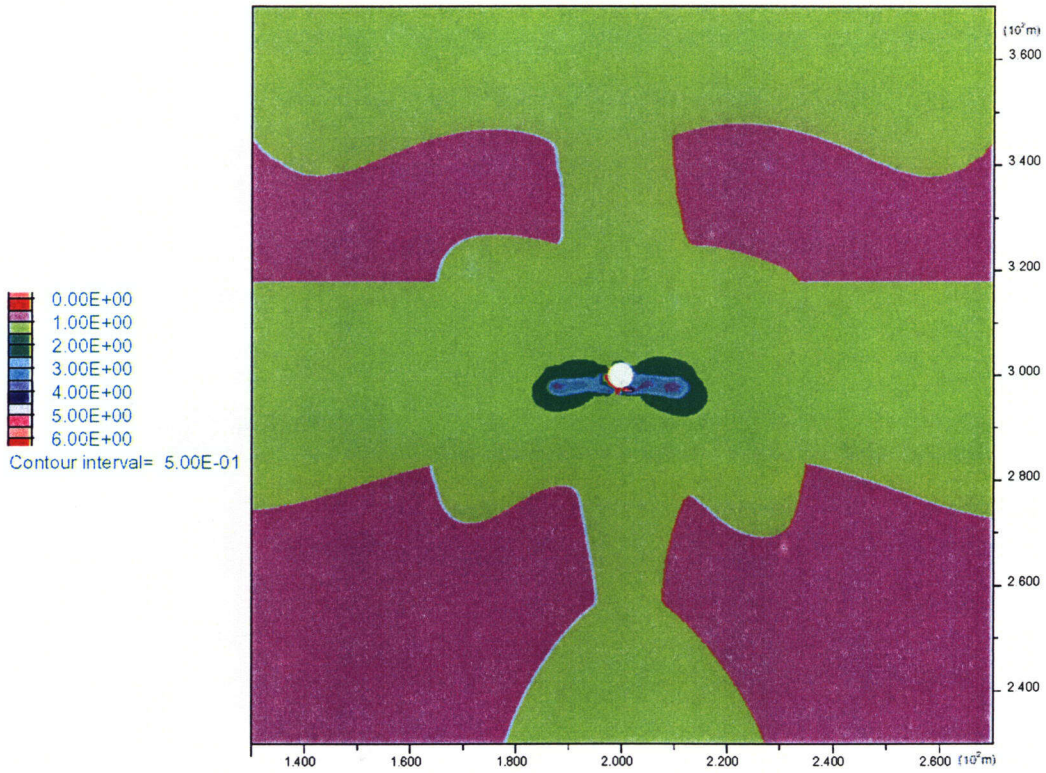

(c) After 4 Years of Heating

Figure 4-38. Permeability variation due to thermally induced deformation for Basecase 2 with Temperature Option 1 (cont'd)

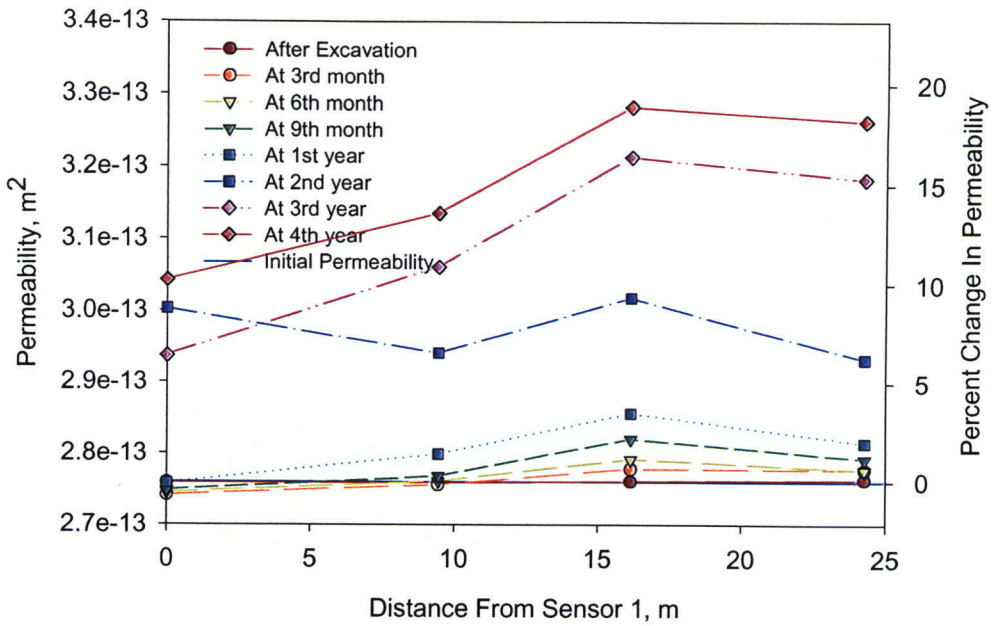

Figure 4-39. Predicted permeability and permeability changes at sensor locations in Hydrologic Hole 57 for Basecase 1 with Temperature Option 1

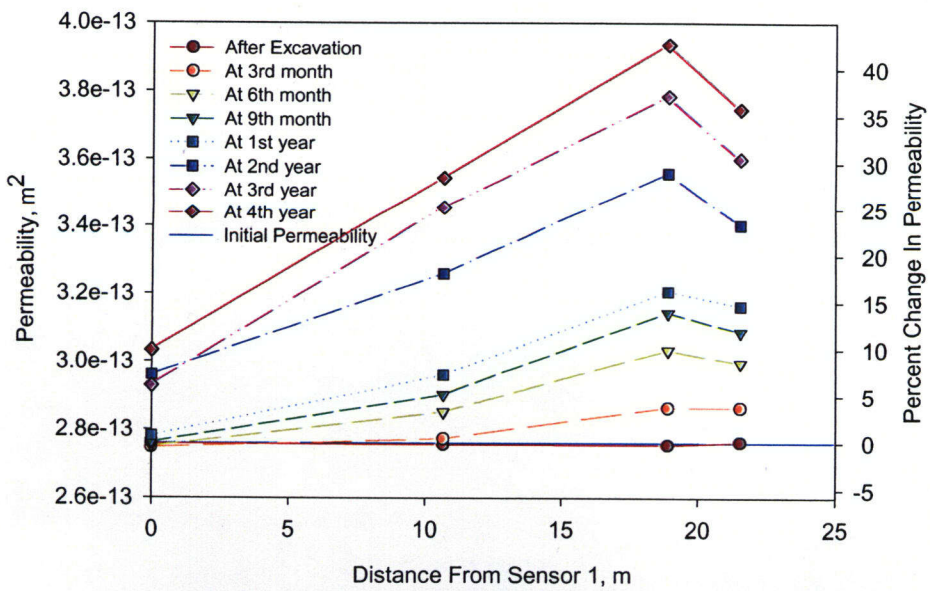

Figure 4-40. Predicted permeability and permeability changes at sensor locations in Hydrologic Hole 59 for Basecase 1 with Temperature Option 1

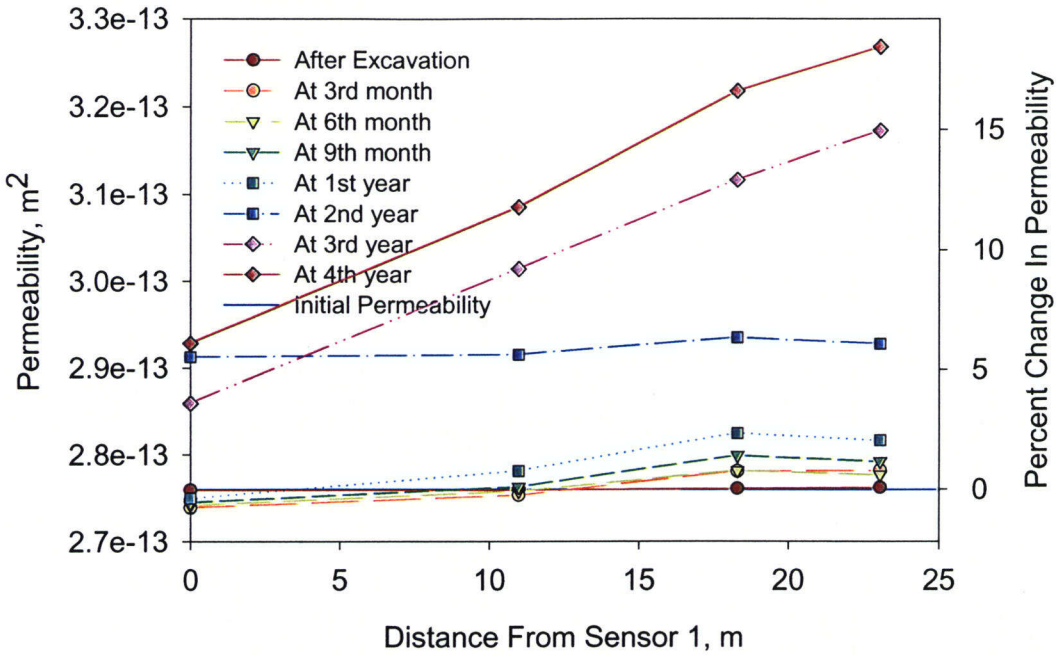

Figure 4-41. Predicted permeability and permeability changes at sensor locations in Hydrologic Hole 74 for Basecase 1 with Temperature Option 1

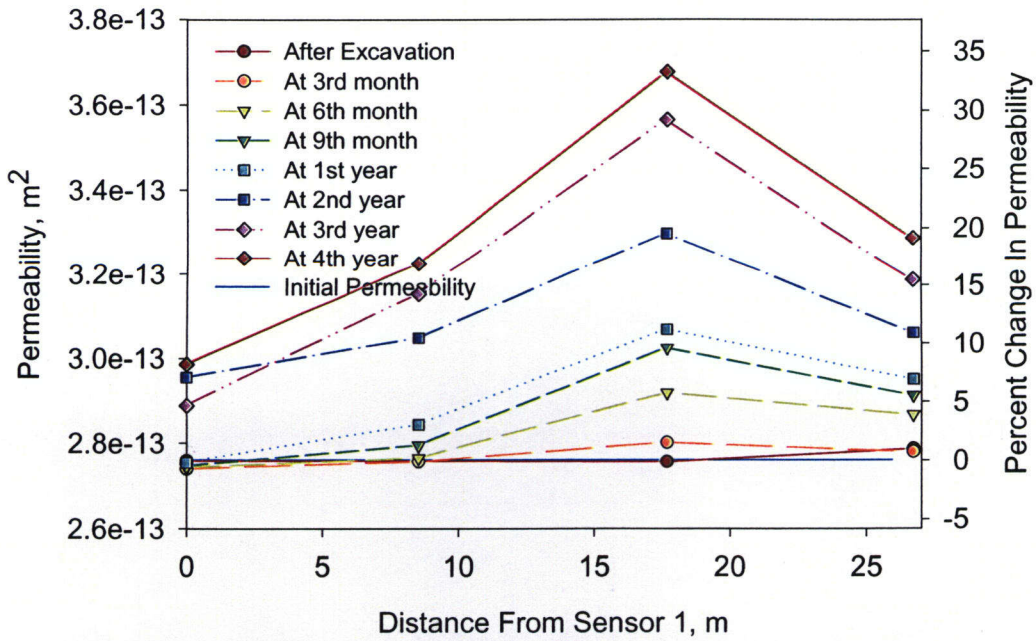

Figure 4-42. Predicted permeability and permeability changes at sensor locations in Hydrologic Hole 76 for Basecase 1 with Temperature Option 1

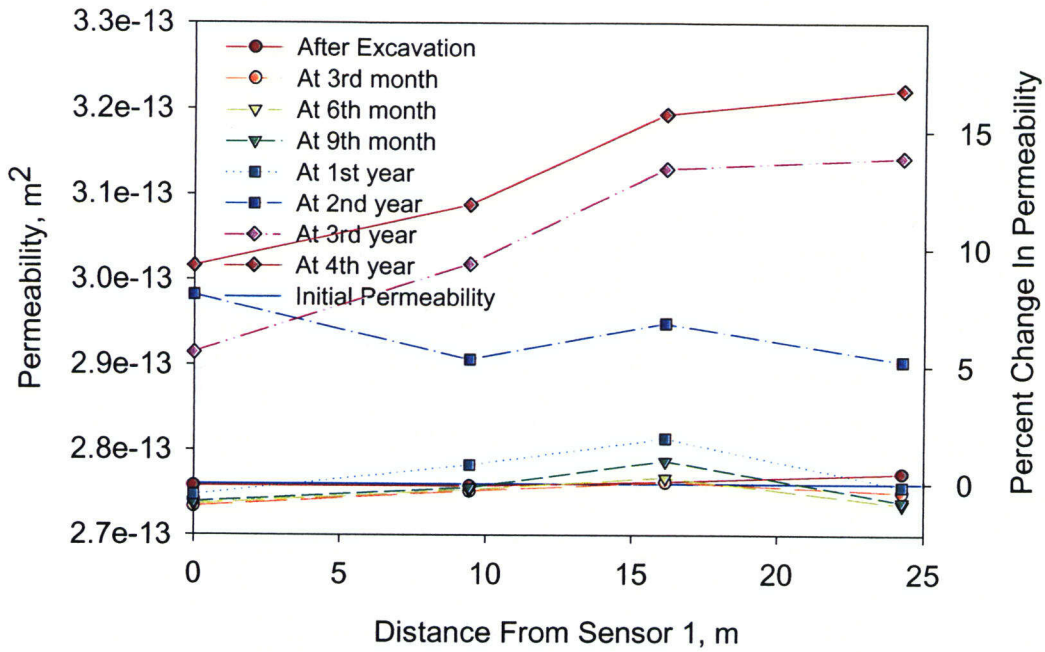

Figure 4-43. Predicted permeability and permeability changes at sensor locations in Hydrologic Hole 57 for Basecase 2 with Temperature Option 1

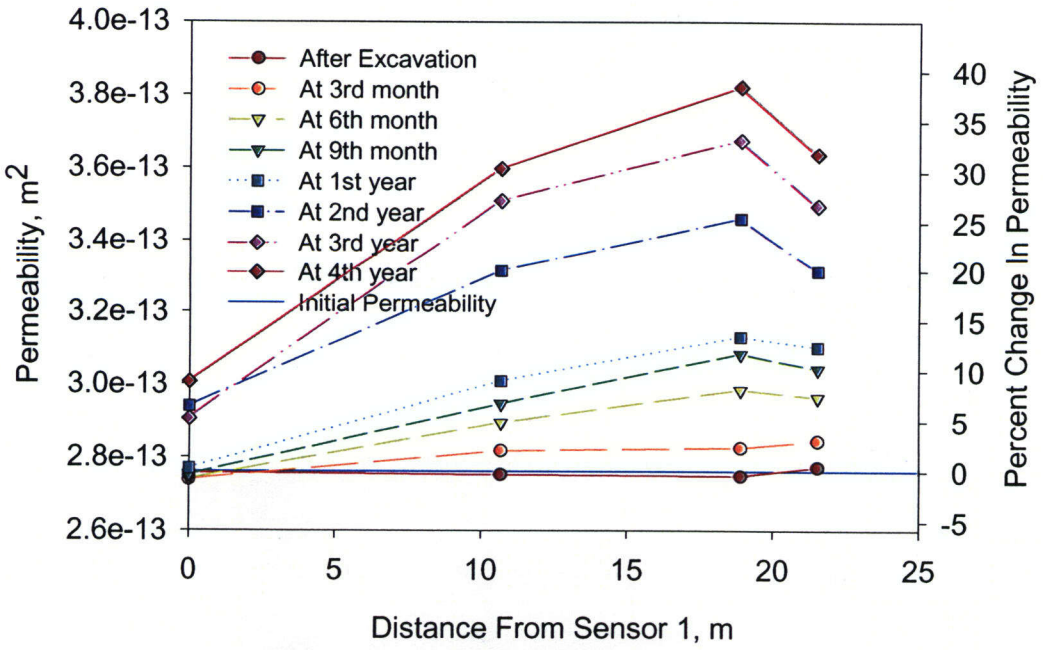

Figure 4-44. Predicted permeability and permeability changes at sensor locations in Hydrologic Hole 59 for Basecase 2 with Temperature Option 1

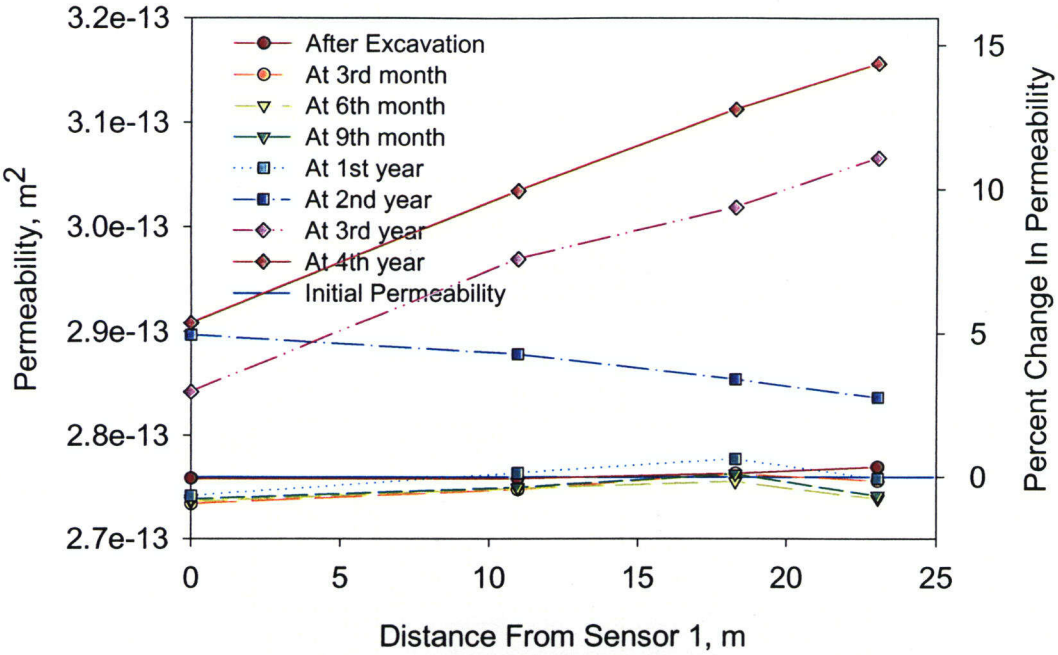

Figure 4-45. Predicted permeability and permeability changes at sensor locations in Hydrologic Hole 74 for Basecase 2 with Temperature Option 1

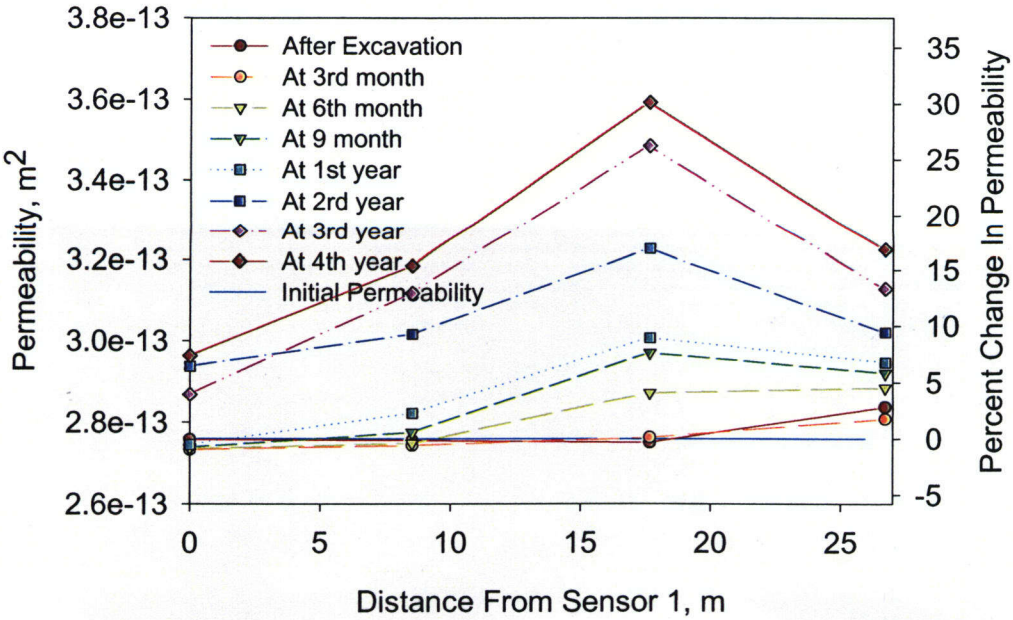

Figure 4-46. Predicted permeability and permeability changes at sensor locations in Hydrologic Hole 76 for Basecase 2 with Temperature Option 1

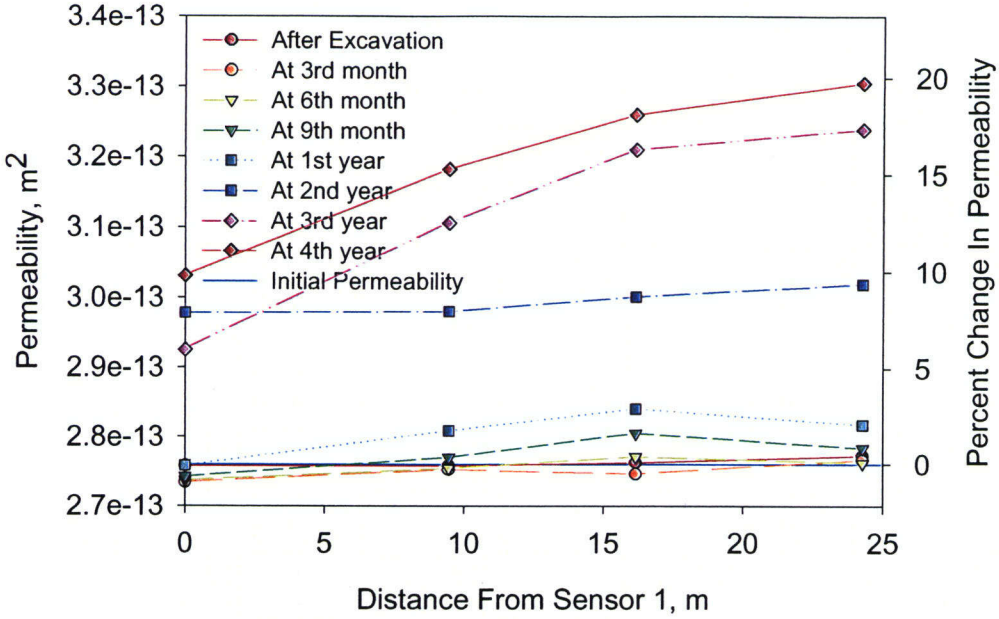

Figure 4-47. Predicted permeability and permeability changes at sensor locations in Hydrologic Hole 57 for Basecase 1 with Temperature Option 2

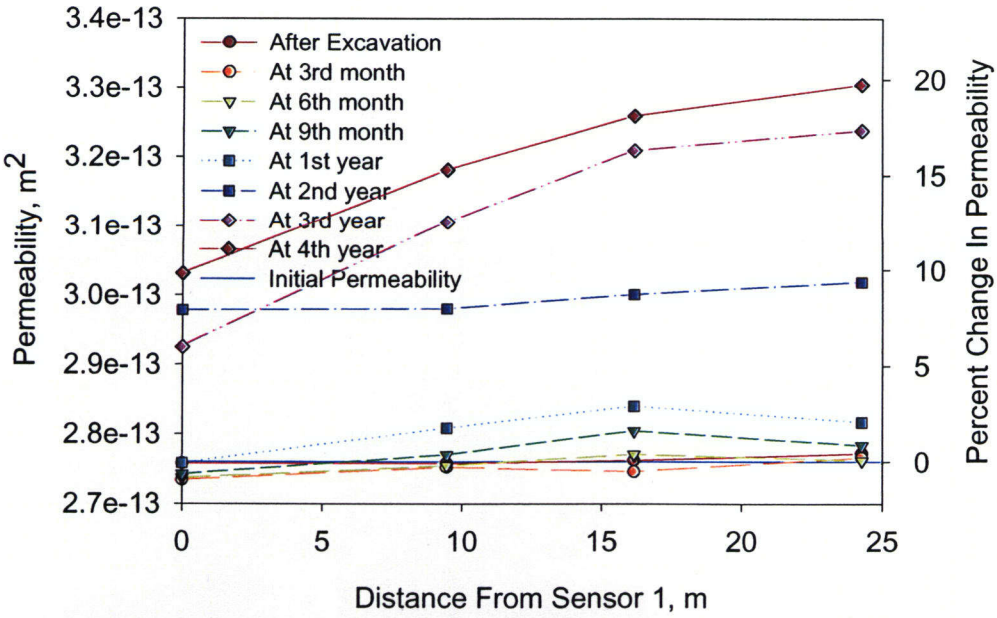

Figure 4-48. Predicted permeability and permeability changes at sensor locations in Hydrologic Hole 59 for Basecase 1 with Temperature Option 2

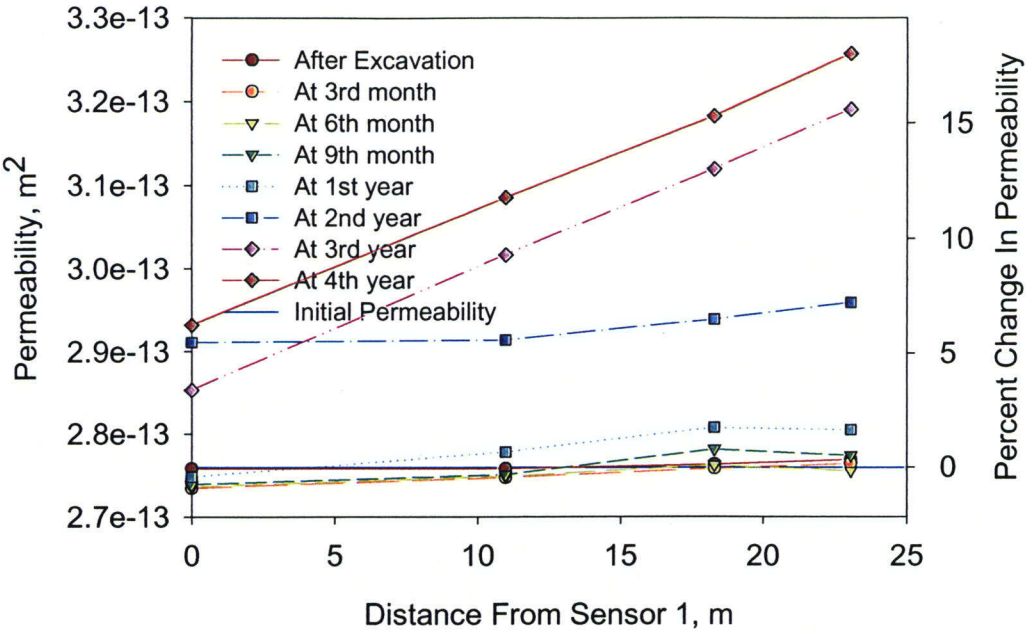

Figure 4-49. Predicted permeability and permeability changes at sensor locations in Hydrologic Hole 74 for Basecase 1 with Temperature Option 2

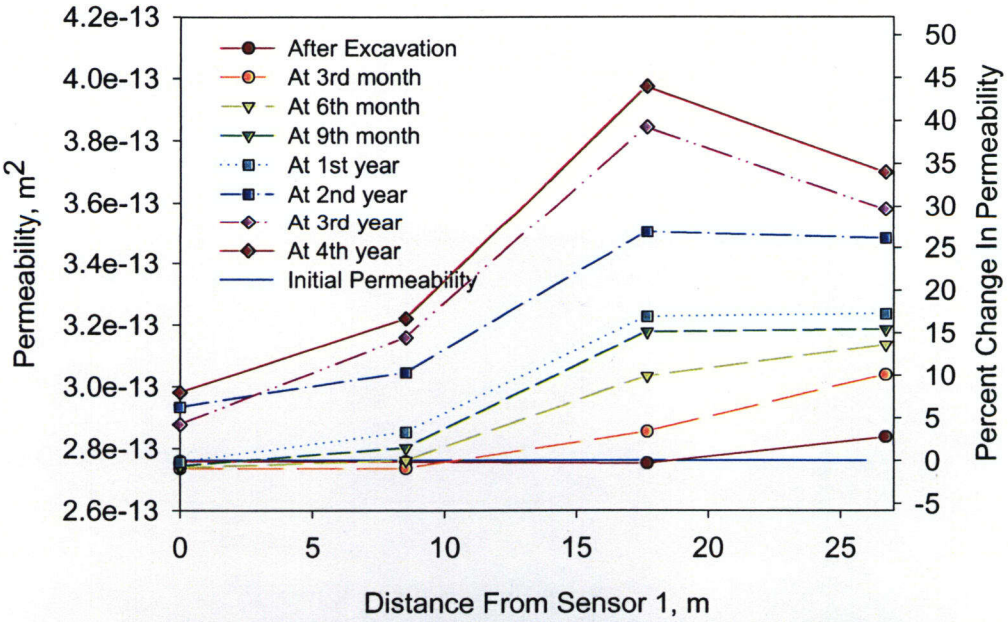

Figure 4-50. Predicted permeability and permeability changes at sensor locations in Hydrologic Hole 76 for Basecase 1 with Temperature Option 2

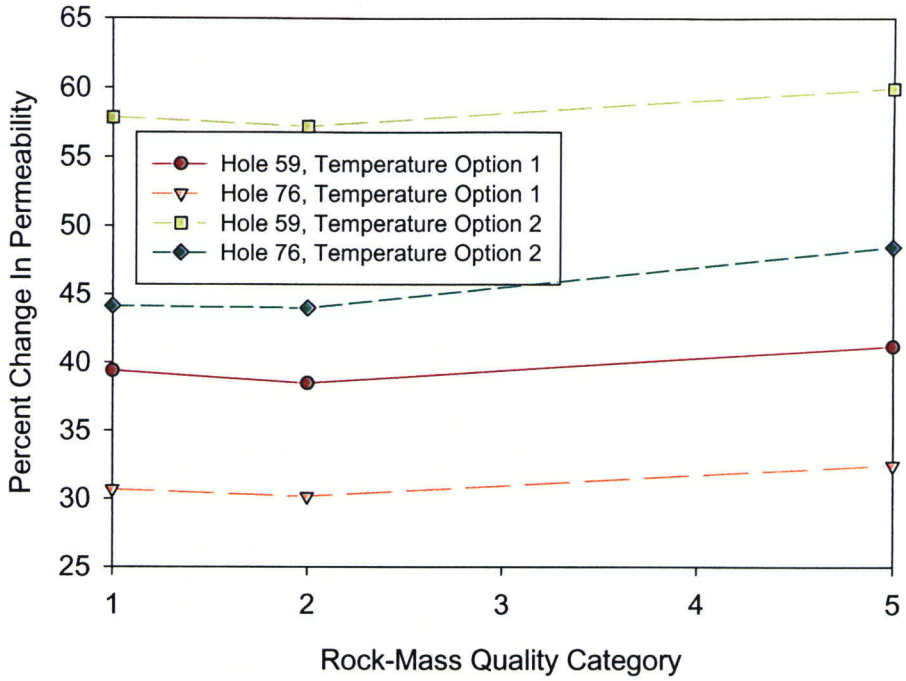

Figure 4-51. The maximum changes predicted in Hydrologic Holes 59 and 76 as a function of rock-mass quality

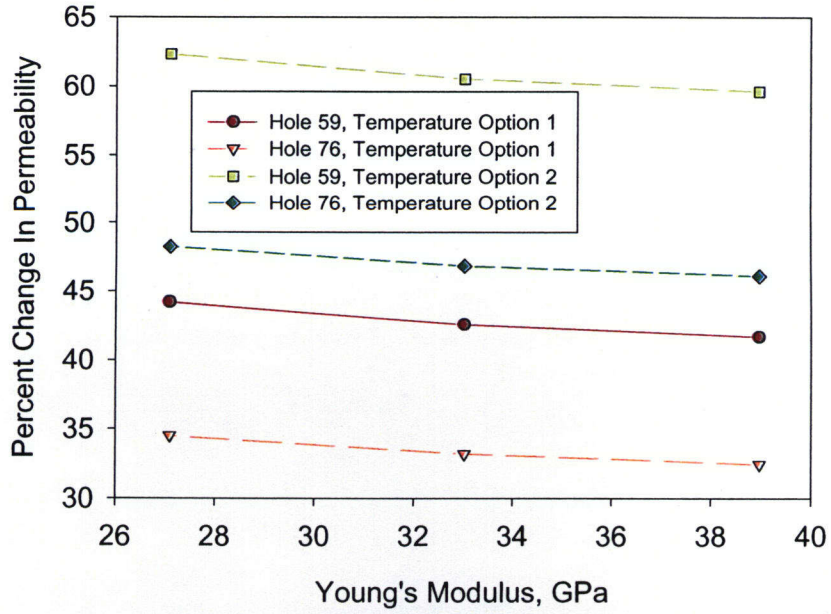

Figure 4-52. The maximum changes predicted in Hydrologic Holes 59 and 76 as a function of Young's modulus

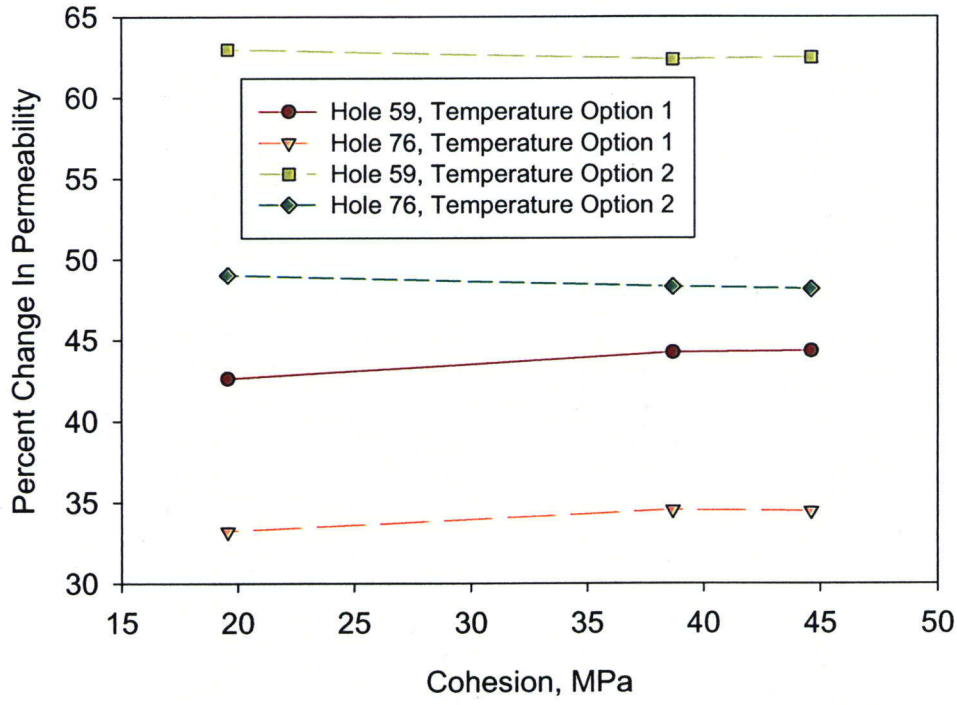

Figure 4-53. Effect of cohesion on permeability change

5 DISCUSSIONS AND SUMMARY

Assessing and developing confidence in the predictive models are important tasks to evaluate the safety case for the geologic repository at Yucca Mountain. The drift-scale heater test at the Exploratory Studies Facility at Yucca Mountain was included in the DECOVALEX III project as a test case to assess the capability of the thermal-mechanical-hydrological-chemical codes to simulate complex thermal-mechanical-hydrological-chemical processes. DECOVALEX III Task 2 contains four subtasks. Subtask 2A is for thermal-hydrological modeling. Both Subtasks 2B and 2C are related to thermal-mechanical modeling, with 2B using the temperature generated in Subtask 2A whereas 2C uses the measured temperatures in the field. Subtask 2D examines thermal-hydrological-chemical modeling. The NRC/CNWRA research team is involved in Subtasks 2A and 2C modeling activities. The activities associated with Subtask 2A, using computer code MULTIFLO, were reported separately. This report was prepared as part of the DECOVALEX III project to independently evaluate FLAC, a thermal-mechanical code used by NRC to support the high-level waste repository program.

The modeling effort for Subtask 2C was to examine rock deformation induced by heating and the thermal-mechanical effect on rock permeability at specific locations. A vertical, cross-sectional two-dimensional model with a regularly structured grid, except in a small region surrounding the drift, was used in this study. This vertical cross section was located at the midspan of the drift and was positioned at a right angle to the drift axis. The fractured rock media were modeled as equivalent continua. Model predictions of thermally induced deformation around the heated drift and the mechanically induced rock permeability variations at specified times and locations will be compared with the corresponding drift-scale heater test measurements when the measured data become available to the Task 2C research teams.

Two basecases were established for the simulations. Basecase 1 modeled the three litho-stratigraphic units with intact rock properties. The mechanical and strength properties used for this case were the mean values adopted from CRWMS M&O (2001). Basecase 2 modeled the three units with equivalent rock-mass properties. The mechanical and strength properties associated with Rock-Mass Quality Category 2 (CRWMS M&O, 2001) were used for this basecase. Besides these two basecases, sensitivity analyses were also conducted to evaluate the effects of variations of Young's modulus and selected strength properties for Basecase 1 and the effects of rock-mass quality for Basecase 2.

Two temperature options were used in this study. Temperature data for Temperature Option 1 were provided by the Task 2 technical monitor research team. The temperature data for Temperature Option 2 were exactly the same as those for Temperature Option 1 except that the location of each temperature value in space was adjusted vertically 2 m [6.56 ft] upward. This adjustment was intended to match better the locations of high-temperature zones with the locations of outer wing heaters.

Thermal-mechanical behavior of fractured rock media can be a complicated process. It is well accepted that, in assessing stability of underground structures, the effects of existing discontinuities should be factored into consideration. In the numerical simulation, these effects may be considered by directly including the discontinuities in the model using the distinct element approach or by indirectly taking into account the discontinuities using the continuum

approach using equivalent rock-mass properties instead of intact rock properties. A continuum modeling approach was adopted in this study.

In this study, both intact rock properties (Basecase 1) and rock-mass properties (Basecase 2) were used in separate analyses for comparison. All the data required for the analyses were provided by the Task 2 technical monitor research team. The differences between the intact-rock and rock-mass properties include reductions in both mechanical and strength properties because a rock mass is weaker than the intact rock or rock block of the same rock type. Considering the basecases only, the rock-mass Young's modulus determined for the Topopah Spring Welded Tuff Unit 1 is approximately 70 percent of the intact rock and approximately 36 percent for the Topopah Spring Welded Tuff Unit 2 (refer to Tables 3-3 and 3-4). The large reduction for the latter is because of its relative higher fracture frequency. The rock-mass cohesion and tensile strength are determined to be approximately 11 percent and 21 percent of the intact rock for the Topopah Spring Welded Tuff Unit 1, and 6 percent and 15 percent for the Topopah Spring Welded Tuff Unit 2. The friction angles for rock-mass and intact rock are essentially the same for both rock units.

Because of the sharp contrast in rock properties, especially in rock strength, between the basecases, it is not surprising for the substantially different deformation responses. The maximum principal stresses experienced in Basecase 1 were considerably higher than those in Basecase 2. The largest difference observed between the two was approximately a factor of 2.5. It was also observed that the tensile stress zone present in Basecase 1 was much larger than in Basecase 2 even though the magnitude was small.

Although the state of stresses in Basecase 1 was high, rock yielding was limited to around both sidewalls and an area above the outer wing heater located at the left side of the heated drift after 4 years of heating; no yielding was found in the rock units either above or beneath the Middle Nonlithophysal unit. As for Basecase 2, besides the yielding in the Middle Nonlithophysal litho-stratigraphic unit as observed in Basecase 1, yielding in the roof and floor of the heated drift was also found. Furthermore, a large extent of yielding was found in the Upper and Lower Lithophysal units above and beneath the Middle Nonlithophysal unit. Yielding conditions, similar to Basecase 2, in the roof of the heated drift and the Upper and Lower Lithophysal units could be induced for Basecase 1 by increasing the Young's modulus or reducing cohesion and tensile strength of the intact rock. However, these yielding conditions were developed at a relatively later stage of heating as compared to those in Basecase 2. This observation is evident by comparing the sizes of the yield zones as shown in Figure 4-10(d) versus Figure 4-18(c) and Figure 4-12(c) versus Figure 4-18(c). In addition, the yielding or failure mode of rock was mostly tensile for analyses using intact-rock properties while shear failure dominated failure mode for analyses using rock-mass properties.

This difference in failure mode is not surprising because of the existence of a large tensile stress zone for the former cases as reported earlier. In addition, the sharp reduction in cohesion for the rock mass as compared to the intact rock makes the shear failure mode much easier to develop in the rock-mass cases than in the intact-rock cases. A crossover from tensile failure dominant to shear failure dominant can be achieved by reducing the Young's modulus and intact rock strength properties simultaneously. A sensitivity analysis (Sensitivity Case 3) showed that, by reducing the properties mentioned in the previous sentence by a standard deviation of the respective mean value used in Basecase 1, yielding observed in the Lower Lithophysal unit

became predominantly shear failure even though the predominant failure mode was still tensile in the Middle Nonlithophysal and Upper Lithophysal units.

The predicted rock displacements at anchor locations of the four multiple-position extensometers relative to the collar of the heated drift, in general, were slightly larger for the cases using rock-mass properties than those using intact rock properties for Temperature Option 1 except for the farthest anchor from the heated drift in multiple-position extensometer boreholes 7 and 8. The predicted displacements in the roof of the heated drift became considerably larger for the cases using rock-mass properties than the ones using intact-rock properties if Temperature Option 2 was used as temperature input.

The predictions in displacement were substantially different between the two temperature options. The predicted values in the roof rock of the heated drift (multiple-position extensometer boreholes 7, 8, and 9) were much larger while the displacements predicted were considerably smaller in the floor rock (multiple-position extensometer borehole 10) for Temperature Option 2 than Temperature Option 1, irrespective of the rock properties used in the analyses. The reason for this difference was not evident because no appreciable difference could be identified in terms of patterns and magnitudes of the maximum and minimum principal stresses and patterns and extent of yield zones. One exception identified was that the yield zone surrounding the heated drift was shifted slightly upward for Temperature Option 2 as compared to Temperature Option 1. This exception might not be sufficient to explain why the predicted roof displacements became larger while the displacements in the floor rock became smaller.

Sensitivity analyses for the intact-rock cases using both temperature options indicated that rock displacement was not very sensitive to the variations of Young's modulus, cohesion, and tensile strength within one standard deviation of the respective mean value. A slight decreasing trend in displacement was observed with increases in Young's modulus.

For rock-mass cases, the predicted displacements in the roof rock increased with increases in Rock-Mass Quality Category designation numbers. A larger designation number indicates higher mechanical and strength properties. This displacement increase is negligible for Temperature Option 1, while it is relatively large for Temperature Option 2.

Considering the pattern of the temperature input, as heating progressed, the horizontal dimension (wall-to-wall) of the heated drift tended to converge (became slightly smaller). The vertical dimension (roof-to-floor) of the heated drift, however, tended to diverge (became slightly bigger). The observed wall-to-wall convergence was more than the roof-to-floor divergence. Temperature options appeared to affect more in the wall-to-wall convergence than the roof-to-floor divergence for all cases using intact-rock properties. The opposite observation was true for all cases using rock-mass properties.

Roof-to-floor divergence and wall-to-wall convergence were found not to be sensitive to the variations of rock properties for the intact-rock cases. An increase in the Rock-Mass Quality Category, however, resulted in an increase in the wall-to-wall convergence for the rock-mass cases.

To assess thermal-mechanical effects on rock permeability, a continuum model representing a deformation-permeability relationship was developed. The fundamental assumptions for this

model included that (i) volumetric strain can be directly related to matrix and fracture porosity changes, (ii) change in matrix permeability is small relative to the change in fracture permeability, and (iii) a fractured rock-mass consists of three mutually perpendicular fracture sets with the same fracture density and aperture. The deformation-permeability model permits an evaluation of deformation-induced permeability increases or decreases. This model has an option to limit the reduction of fracture porosity to a predetermined residual value beyond which the fracture porosity is no longer compressible. This model was used in the Task 2C study to predict thermal-mechanically induced permeability variations. The predicted results at specified locations will be compared with the field-measured values to evaluate this deformation-permeability model at a later time when the measured data are provided by the Task 2 technical monitor research team.

The results of the case studies indicated that, after excavation, a slight decrease in permeability could be observed in a large region surrounding the drift. The change amounted to no more than 20 percent of reduction to the initial permeability. Significant reduction in permeability in a small region at the lower-left corner of the drift was found for all cases analyzed. This irregularity could be attributed to an artifact of the irregular grid structure near the drift and is judged to have no appreciable effects on the thermal-mechanically induced permeability variations in a relatively large scale as studied here.

The excavation-induced permeability deficits in all cases studied were overcome at the early stage of heating. The increase in permeability caused by heating was found to be large in scale. The largest increases were identified in areas coinciding with the highest temperature zones. As heating progressed, these areas with high permeability change expanded outward from the high-temperature zones because of the spreading of the high-temperature zones themselves. The dimensions of the regions with the permeability twice the initial value were approximately two drift-diameters wide and one drift-diameter high. The regions were located on both sides of the heated drift.

Permeability variations were predicted in the four selected hydrologic pressure sensor holes. Among them, Hydrologic Holes 57 and 59 were located at a cross section approximately 10 m [32.1 ft] and Hydrologic Holes 74 and 76 at a location approximately 30 m [98.4 ft] from the thermal bulkhead. Hydrologic Holes 59 and 76 were closer to the wing heaters between the observation drift and the heated drift than the other holes with Hydrologic Hole 59 being the closest. As a result, the permeability predicted because of thermal-mechanical effect was the highest for the sensors in Hydrologic Hole 59.

The permeability increases predicted for the intact-rock cases were higher than those for the rock-mass cases. However, the difference was insignificant. Also, the predicted permeability changes were not sensitive to the variations of rock properties for the intact-rock cases nor to the rock-mass quality for the rock-mass cases.

Temperature options were found to have more influence on permeability prediction than the variations in rock-mass quality and intact-rock properties. The predicted largest permeability increase for Temperature Option 2 after 4 years of heating was approximately 61 percent for at the location of Sensor 3 of Hydrologic Hole 49 for the intact-rock basecase and was approximately 20 percent more than that for Temperature Option 1. This magnitude of change

in permeability is considered to be inconsequential, considering the relatively large uncertainty associated with *in-situ* permeability measurements.

6 REFERENCES

Barton, N.R., R. Lien, and J. Lunde. "Engineering Classification of Rock Masses for the Design of Tunnel Support." *Rock Mechanics*. Vol. 6, No. 4. pp. 189–239. 1974.

Bandis, S.C., A.C. Lumsden, and N.R. Barton. "Fundamentals of rock joint deformation." *International Journal of Rock Mechanics and Mining Sciences & Geomechanics Abstracts*. Vol. 20, No. 6. pp. 249–368. 1983.

Barton, N.R., S.C. Bandis, and K. Bakhtar. "Strength, deformation, and conductivity coupling of rock joints." *International Journal of Rock Mechanics and Mining Sciences & Geomechanics Abstracts*. Vol. 22, No. 3. pp. 121–140. 1985.

Bieniawski, Z.T. "Rock Mass Classification in Rock Engineering." *Exploration for Rock Engineering*. Z.T. Bieniawski, ed. Vol. 1. pp. 97–106. Cape Town, South Africa: A.A. Balkema. 1976.

Bieniawski, Z.T. *Engineering Rock Mass Classifications*. New York City, New York: Wiley and Sons. 1989.

CRWMS M&O. "Ambient Characterization of the Drift-Scale Test Block." BADD00000–01717–5705–00001. Rev. 01. Las Vegas, Nevada: CRWMS M&O. 1997a.

———. "Drift Scale Test Design and Forecast Results." BAB000000–01717–4600–00007. Rev. 01. Las Vegas, Nevada: CRWMS M&O. 1997b.

———. "Yucca Mountain Site Geotechnical Report." B00000000–01717–5705–00043. Vol. 1. Rev. 01. Las Vegas, Nevada: CRWMS M&O. 1997c.

———. "Drift Scale Test As-Built Report." B00000000–01717–5700–00003. Rev. 01. Las Vegas, Nevada: CRWMS M&O. 1998.

———. "TBV-332/TBD-325 Resolution Analysis: Geotechnical Rock Properties." B00000000–01717–5705–00134. Rev. 00. Las Vegas, Nevada: CRWMS M&O. 1999.

———. "Multiscale Thermohydrologic Model." ANL–EBS–MD–000049. Rev. 00 ICN 02. Las Vegas, Nevada: CRWMS M&O. 2001.

Elsworth, D. "Thermal Permeability Enhancement of Blocky Rocks: One-Dimensional Flow." *International Journal of Rock Mechanics and Mining Sciences & Geomechanics Abstracts*. Vol. 26, No. 3/4. pp. 329–339. 1989.

Elsworth, D. and C.R. Mase. "Chapter 8: Groundwater in Rock Engineering." *Comprehensive Rock Engineering* 1. J.A. Hudson, ed. New York City, New York: Pergamon Press. pp. 201–226. 1993.

Green, R.T., M.E. Hill, and S.L. Painter. "Progress Report for DECOVALEX III Task 2: Numerical Simulation of the Drift-Scale Heater Test at Yucca Mountain." San Antonio, Texas: CNWRA. 2001.

Hsiung, S.M., D.D. Kana, M.P. Ahola, A.H. Chowdhury, and A. Ghosh. NUREG/CR–6178, "Laboratory Characterization of Rock Joints." Washington, DC: NRC. 1994.

Lichtner, P.C., M.S. Seth, and S. Painter. "MULTIFLO User's Manual MULTIFLO Version 1.2—Two-Phase Nonisothermal Coupled Thermal-Hydrologic-Chemical Flow Simulator." Reversion 2. Change 1. San Antonio, TX: Center for Nuclear Waste Regulatory Analyses. 2000.

Mohanty, S., A.H. Chowdhury, S.M. Hsiung, and M.P. Ahola. "Single Fracture Flow Behavior of Apache Leap Tuff Under Normal and Shear Loads." CNWRA 94–024. San Antonio, Texas: CNWRA. 1994.

Ofoegbu, G.I. "Variations of drift at the proposed Yucca Mountain repository." Rock Mechanics for Industry. Proceedings of the 37th U.S. Rock Mechanics Symposium. B. Amadei, R.L. Kranz, G.A. Scott, and P. Smeallie, eds. Rotteram, The Netherlands: A.A. Balkema. pp. 767–773. 1999.

Ofoegbu, G.I. "Thermal-Mechanical Effects on Long-Term Hydrological Properties at the Proposed Yucca Mountain Nuclear Waste Repository." CNWRA 2000-03. San Antonio, Texas: CNWRA. 2000.

Panda, M.N., and L.W. Lake. "Estimation of single-phase permeability from the parameters of a particle-size distribution. *AAPG Bulletin*. Vol. 78, No. 7. pp. 1,028–1,039. 1994.

Schrauf, T.W. and D.D. Evans. "Laboratory Studies of Gas Flow Through a Single Natural Fracture." *Water Resources Research*. Vol. 22, No. 7. pp. 1,038–1,050. 1986.

Witherspoon, P.A., J.S.Y. Wang, K. Iwai, and J.E. Gale. "Validity of Cubic Law for Fluid Flow in a Deformation Rock Fracture." *Water Resources Research*. Vol. 16, No. 6. pp. 1,016–1,024. 1980.